

# Dynamics near a periodically-perturbed robust heteroclinic cycle

Tsung-Lung Tsai

*Department of Mathematics, National Changhua University of Education,  
Jin-De Campus, Changhua, Taiwan 500, R.O.C. [ttloug23@cc.ncue.edu.tw](mailto:ttloug23@cc.ncue.edu.tw)*

and

Jonathan H. P. Dawes

*Department of Mathematical Sciences, University of Bath,  
Claverton Down, Bath BA2 7AY, UK. [J.H.P.Dawes@bath.ac.uk](mailto:J.H.P.Dawes@bath.ac.uk)*

Date: July 8, 2013

## Abstract

Robust heteroclinic cycles (RHCs) arise naturally in collections of symmetric differential equations derived as dynamical models in many fields, including fluid mechanics, game theory and population dynamics. In this paper, we present a careful study of the complicated dynamics generated by small amplitude periodic perturbations of a stable robust heteroclinic cycle (RHC). We give a detailed derivation of the Poincaré map for trajectories near the RHC, asymptotically correct in the limit of small amplitude perturbations. This reduces the nonautonomous system in  $\mathbb{R}^3$  to a 2D map.

We identify three distinct dynamical regimes. The distinctions between these regimes depend subtly on different distinguished limits of the two small parameters in the problem. The first regime corresponds to the RHC being only weakly attracting: here we show that the system is equivalent to a damped nonlinear pendulum with a constant torque. In the second regime the periodically-perturbed RHC is more strongly attracting and the system dynamics corresponds to that of a (non-invertible or invertible) circle map. In the third regime, of yet stronger attraction, the dynamics of the return map is chaotic and no longer reducible to a one-dimensional map. This third regime has been noted previously; our analysis in this paper focusses on providing quantitative results in the first two regimes.

## 1 Introduction

A heteroclinic cycle in a dynamical system consists of saddle-type invariant sets (equilibrium points, periodic orbits or chaotic attractors), and heteroclinic trajectories connecting them. In generic dynamical systems without symmetry or other constraints, such configurations are structurally unstable. On the other hand, in symmetric systems the existence of invariant subspaces (fixed under a symmetry subgroup) may force the existence of such connecting trajectories; heteroclinic cycles may then become robust in the sense that the heteroclinic cycle persists under small symmetry-preserving perturbations.

Examples of robust heteroclinic cycles (RHCs) connecting equilibrium points have been discussed in many contexts [28, 17, 24, 10, 12, 7, 31]. Perhaps the most important motivations for their study have been ecological models of competing species [18, 28], thermal convection [9, 6, 34], game theory [14, 38], and mathematical neuroscience [35, 44, 42, 37, 43, 3, 4, 36]. In biological settings, systems with heteroclinic cycles represent mathematically the concept of ‘winnerless competition’ which has been widely discussed as being a more biologically-relevant paradigm than the alternative ‘winner-takes-all’ assumption in many scenarios, especially in game theory and evolutionary biology [30].

The focus of this paper is on the specific, seemingly simple model problem given by the following set of three ordinary differential equations:

$$\begin{cases} \dot{x} &= x(1 - (x + y + z) - cy + ez) + \gamma(1 - x)f(2\omega t) \\ \dot{y} &= y(1 - (x + y + z) - cz + ex) \\ \dot{z} &= z(1 - (x + y + z) - cx + ey) \end{cases}. \quad (1)$$

In the case  $\gamma = 0$  this is exactly the toy model example proposed by May and Leonard in 1975 [28] as an example of competitive Lotka–Volterra type model for the dynamics of three populations:  $x(t)$ ,  $y(t)$  and  $z(t)$  are the non-negative proportions of the total population that consists of each species. May and Leonard proved that when the coefficients satisfy  $0 < e < c < 1$ , there exists an attracting invariant set in the closed octant  $\mathbb{R}_+^3$  that consists of three saddle-type equilibrium points, situated one on the positive part of each axis, and heteroclinic connecting orbits between them. The dynamical behaviour is aperiodic: typical trajectories near this ‘heteroclinic cycle’ spend increasing amounts of time near each saddle point on each occasion that they return close to it. Although May and Leonard did not point out the robustness of this cycle, it clearly is robust due to an obvious biological constraint (in the case  $\gamma = 0$ ): if a species is extinct at time  $t = 0$ , it will remain extinct for all  $t > 0$ . In other words, the coordinate planes  $\{x = 0\}$ ,  $\{y = 0\}$  and  $\{z = 0\}$  form invariant planes supporting the connecting orbits. Within each of these invariant planes the relevant connecting orbit is a saddle-sink connection, and therefore it is structurally stable.

Guckenheimer and Holmes [17] analysed the May–Leonard example further and confirmed more generally that robust heteroclinic cycles exist in open subsets of the space of  $C^r$  vector fields,  $r \geq 1$ , on  $\mathbb{R}^3$  which are equivariant with respect to a symmetry group generated by two elements, namely, cyclic permutation of the coordinate axes and reflection in the coordinate planes.

Symmetry-breaking constant perturbations to RHCs are well-known [21] to result in long-period periodic orbits that lie close to the original cycle. For a heteroclinic cycle perturbed by random noise, the time taken for trajectories to return to a cross section transverse to the original heteroclinic cycle becomes a random variable with well-defined statistics, for example the mean return time [40]. Perhaps surprisingly, given these previous studies, to date there has been very little systematic investigation of the effects of perturbations that are time-periodic, despite that being natural for the modelling of many biological effects. Mathematically, one might expect to make comparisons between the effects of time-periodic forcing on a heteroclinic cycle and the well-known effects of time-periodic forcing on periodic oscillations, for example frequency-locking. These general observations provide twin motivations for the work described in this paper.

In this paper we consider the extension of the Lotka–Volterra type model (1) taking  $f(2\omega t)$  to be a non-negative,  $2\pi$ -periodic and continuously differentiable function, and the perturbation amplitude  $\gamma$  to be small and positive:  $0 < \gamma \ll 1$ . Our choice of perturbation term, and its appearance only in one coordinate is made for two reasons. First, it simplifies the quantitative reduction of the differential equations to a map, as we outline in section 2.3 and in the Appendix. Second, it allows comparison with previous work by other authors, in particular Rabinovich et al. [35].

Considering the form of the periodic forcing, the choices made in (1) are a generalized version of the system studied in [35]. There, the motivation was neuronal dynamics, and so the variables  $x(t)$ ,  $y(t)$ ,  $z(t)$  represented instantaneous firing rates of neuronal circuits within each of which couplings are assumed to be stronger than the couplings between circuits. In this context Rabinovich et al [35] used the dynamics of (1) to examine possible synchronisation phenomena in the ‘winnerless competition’ between three neural circuits. For example, they reported numerically the existence of a sequence of intervals in the forcing frequency  $\omega$  within which frequency locking is observed (for the specific case  $c = 0.25$ ,  $e = 0.2$  and  $f(2\omega t) = \sin^2(\omega t)$ ) and outside which complicated dynamics are observed. Since in this case the dynamical variables represent firing rates they are clearly non-negative quantities, and the form of the perturbation term was chosen to preserve this feature. This is also a sensible feature in terms of the population dynamics motivation of May and Leonard. But mathematically, other choices are of course

possible and may lead to more complex behaviour. We leave these further possibilities as the subject of future work, expecting that the results we present here are useful in this wider context.

In our previous papers [13, 41] we presented preliminary results of investigations. We pointed out the existence of two distinct dynamical regimes corresponding to the existence or non-existence of intervals of frequency locking as  $\omega$  varies. The present paper substantially extends and generalises these results: we highlight the existence of a third regime, in which the dynamics can be reduced to that of a damped nonlinear pendulum; we provide substantial additional detail on the intermediate regime in which the dynamics is equivalent to a circle map; and we carry out quantitative analyses in the invertible and non-invertible cases. The Appendix contains the construction of the Poincaré map for general  $f(2\omega t)$ ; the paper [13] worked exclusively with the case  $f(2\omega t) = \sin^2(\omega t)$ .

We now briefly describe the main results and the contents of this paper. Our approach is asymptotic in nature and throughout the analysis we consider the amplitude  $\gamma$  of the time-periodic perturbation to be sufficiently small that terms of  $O(\gamma^2)$  and higher can be neglected. A second parameter of considerable interest is  $\epsilon := (c/e)^3 - 1$  which measures the attractivity of the RHC. The forcing frequency  $\omega$  is our principal bifurcation parameter, and in several places we consider limits of small and large  $\omega$  in order to make analytic progress. In section 2, we review the definition of RHCs, the symmetric dynamics context and we summarise the effect of adding constant symmetry-breaking perturbations, in order to set the scene. In section 2.3, we present the Poincaré map of the system (1) for the case  $f(2\omega t) = \sin^2(\omega t)$ . The Poincaré map for this non-autonomous system yields a description of the dynamics in terms of a 2D map for the  $x$ -coordinate and the return time  $t$  at which trajectories cross the Poincaré section. Although one might expect the  $x$ -coordinate of the map to decay rapidly until it is of the same asymptotic order as the perturbation amplitude  $\gamma$ , careful investigation of the dynamics is necessary to make this statement precise; the existence of two small parameters allows a distinguished limit to arise in which this is not the case. Section 2.4 considers the interaction between these two small parameters in detail and defines the ‘weakly attracting’ and ‘strongly attracting’ regimes. Having introduced the parameter  $\epsilon$  that measures the rate of convergence of trajectories to the RHC that exists in the unperturbed case  $\gamma = 0$ , we describe the ‘weakly attracting’ case that arises in the distinguished limit  $\gamma \ll 1$  such that  $\gamma^\epsilon \sim 1$ , and the ‘strongly attracting’ case that arises in the limit  $\gamma \ll 1$  such that  $\gamma^\epsilon \ll 1$ . We also informally refer to the weakly attracting case as being ‘ $\epsilon$  near 0’ and the strongly attracting case as being ‘ $\epsilon$  of order unity’; implicitly we consider  $\gamma$  always to be asymptotically small.

We discuss these two cases in detail in sections 3 and 4, respectively, which are the heart of the paper. In section 3 we show that in the weakly attracting case the dynamics of the Poincaré map is equivalent to the well-known two-dimensional continuous time dynamics of a forced damped pendulum with torque. For this problem trajectories are attracted generically either to a stable equilibrium, or to a stable periodic orbit. For an open region of parameter space these two stable invariants coexist: the dynamics exhibit bistability. The implication of these results for our forced RHC are that, for a fixed forcing frequency, there are three possible attracting sets: a periodic orbit, a stable 2-dimensional torus, or their coexistence within a region of bistability.

In section 4, where the RHC is strongly attracting, we observe circle map dynamics. We show in section 4 that the system is equivalent (i) to an invertible circle map when the forcing frequency  $\omega$  is large, and (ii) to a non-invertible circle map when  $\omega > 0$  is sufficiently small. For intermediate values of  $\omega$  we are unable to proceed analytically due to the complicated form of the Poincaré map. We provide numerical evidence that the transition from a non-invertible to an invertible circle map when  $\omega$  increases is ‘monotonic’ in the sense that there is a single value of the forcing frequency above which no chaotic dynamics appears, but below which every interval in which the dynamics appears to be complicated appears to contain chaos.

Section 5 contains additional results that set the paper in a wider context. In subsection 5.1 we compare our results with the results of Afraimovich et al [2], who also carried out a derivation of the Poincaré map for a periodically-perturbed Lotka–Volterra-type system in  $\mathbb{R}^3$  and investigated the bifurcation structure analytically. The results of [2] agree with, and are complementary to, those we present here. Afraimovich

et al. [2] establish sufficient conditions for the dynamics of the periodically forced RHC to be either ‘regular’ (i.e. having an invariant closed curve as the maximal attractor) or chaotic in the sense that the dynamics of the 2D return map is chaotic. The regular regime corresponds to our strongly attracting regime in which the dynamics are those of a circle map. Since we keep the forcing frequency  $\omega$  as an explicit bifurcation parameter, we are able to probe the structure of the strongly attracting regime in more detail. We remarked on the existence of the chaotic regime for the 2D return map in our previous paper [13], see in particular figure 6 in that paper. Given this, the detailed work we present on the weakly and strongly attracting regimes, and the sufficient condition for chaotic dynamics deduced by [2], we do not comment further on this third regime in the present paper.

In section 5.2 we briefly discuss more general classes of periodic perturbation. In many respects the dynamics of the Poincaré map of the ODE system (1) for the case  $f(2\omega t) = \sin^2(\omega t)$  turn out to be indicative of the dynamics of the system (1) for general periodic functions  $f(2\omega t)$ . However, the perturbation function  $\gamma \sin^2(\omega t)$  has the particular feature that its time-average and maximum amplitude are of the same order. Clearly it is of interest to explore cases where the mean and maximum amplitude of the forcing function  $\gamma f(2\omega t)$  do not scale in the same way. In section 5.2 we propose a slightly more general form for the forcing function in order to derive a generalised model map; we then briefly discuss its bifurcation structure. We summarise our results in section 6.

## 2 Symmetric structure and perturbation effects

In this section we recall and summarise standard definitions from equivariant dynamics and introduce our model example.

### 2.1 Symmetric structure

Let  $\Gamma \in \mathbf{O}(n)$  be a compact Lie group acting linearly on  $\mathbb{R}^n$ . Let  $f : \mathbb{R}^n \rightarrow \mathbb{R}^n$  be a  $\Gamma$ -equivariant vector field. That is

$$f(\gamma x) = \gamma f(x), \quad \forall \gamma \in \Gamma \quad \text{and} \quad \forall x \in \mathbb{R}^n.$$

**Definition 2.1** *Suppose that  $\xi_j, j = 1, \dots, m$  are hyperbolic equilibria of the vector field  $f(x)$  and that the group orbits  $\Gamma \xi_j = \{\gamma \xi_j : \gamma \in \Gamma\}, j = 1, 2, \dots, m$  are distinct. Let  $W^s(\xi_j)$  and  $W^u(\xi_j)$  denote the stable and unstable manifolds of  $\xi_j$ , respectively. The set of group orbits of the unstable manifolds*

$$X = \{W^u(\gamma \xi_j), j = 1, \dots, m, \gamma \in \Gamma\}$$

*is said to form a heteroclinic cycle provided  $\dim W^u(\xi_j) = 1$  for all  $j = 1, \dots, m$  and*

$$W^u(\xi_j) - \{\xi_j\} \subset \bigcup_{\gamma \in \Gamma} W^s(\gamma \xi_{j+1}).$$

*Here, we use indices ‘modulo  $m$ ’, i.e. we set  $m+1 \equiv 1$ . If  $m = 1$ , we call  $X$  a homoclinic cycle.*

Let  $\Sigma \subseteq \Gamma$  be a subgroup. We define its fixed-point subspace by

$$\text{Fix}(\Sigma) = \{x \in \mathbb{R}^n : \sigma x = x, \forall \sigma \in \Sigma\}.$$

In particular, since  $f(\text{Fix}(\Sigma)) \subset \text{Fix}(\Sigma)$  for every  $\Gamma$ -equivariant  $f$  and isotropy subgroup  $\Sigma$ , the following definition is natural:

**Definition 2.2** *The heteroclinic cycle  $X$  is a robust heteroclinic cycle if for each  $j = 1, \dots, m$ , there exists a fixed-point subspace  $P_j = \text{Fix}(\Sigma_j)$  where  $\Sigma_j \subset \Gamma$ , such that (i)  $\xi_{j+1}$  is a sink in  $P_j$  (considering indices to be taken ‘modulo  $m$ ’ as before) and (ii)  $W^u(\xi_j) \subset P_j$ .*

In [17] Guckenheimer and Holmes considered  $\Gamma$ -equivariant vector fields for the group  $\Gamma \subset \mathbf{O}(3)$  generated by

$$r_x = \begin{pmatrix} -1 & 0 & 0 \\ 0 & 1 & 0 \\ 0 & 0 & 1 \end{pmatrix} \quad \text{and} \quad \sigma = \begin{pmatrix} 0 & 0 & 1 \\ 1 & 0 & 0 \\ 0 & 1 & 0 \end{pmatrix},$$

i.e.  $\Gamma$  consists of cyclic permutations of the coordinate axes in  $\mathbb{R}^3$  and reflections in the coordinate planes. It is easily shown that systems of  $k$ -times continuously differentiable ODEs ( $k \geq 3$ ) that are equivariant with respect to  $\Gamma$  have a truncated Taylor expansion at the origin that takes the form (up to cubic order)

$$\begin{cases} \dot{x} = x(\lambda + a_1x^2 + a_2y^2 + a_3z^2) \\ \dot{y} = y(\lambda + a_1y^2 + a_2z^2 + a_3x^2) \\ \dot{z} = z(\lambda + a_1z^2 + a_2x^2 + a_3y^2) \end{cases}, \quad (2)$$

which we will refer to as the ‘G–H system’ of ODEs. The G–H system is closely related to the Lotka–Volterra system (1), with  $\gamma = 0$  through the change of variables  $(\tilde{x}, \tilde{y}, \tilde{z}) = (x^2, y^2, z^2)$ . To put the ODEs into exactly the form (1) it is necessary also to carry out a rescaling of time and the dependent variables in order to set  $\lambda = a_1 = 1$ . Finally, we note that the non-negativity of the forcing term ensures that the positive orthant remains forward-invariant under time integration so we may restrict our attention to that part of the phase space.

Removing this restriction, and considering a forcing term that took both positive and negative values, would be most natural in the context of the G–H system (2) rather than for the Lotka–Volterra version (1) due to the change of variables that relates them. We expect that a forcing term taking values of both signs added to the G–H system would lead to switching near to the heteroclinic network formed by the group orbits of equilibria. This would demand a more detailed analysis, keeping track of which equilibrium points a trajectory had visited. We would expect this paper to provide useful material to support the investigation of the dynamics in this, more complex, situation which we may consider in future work.

Throughout the paper we consider the coefficients to satisfy  $0 < e < c < 1$  which guarantees the existence of an asymptotically stable robust heteroclinic cycle when  $\gamma = 0$ .

## 2.2 Effects of perturbations

Additive constant perturbations to (2) or the Lotka–Volterra version (1) with  $\gamma = 0$ , usually result in long-period periodic orbits that lie close to the RHC that exists when the perturbation is not present. This observation is widely recognised in the literature, for example see Proctor & Jones [34] and Krupa [21]. The period of the periodic orbit is ‘long’ in the sense that it tends to infinity as the amplitude of the perturbation tends to zero, usually logarithmically:  $T \sim \tilde{C}_1 \log(1/\gamma)$  where  $\gamma$  is a (positive) measure of the amplitude of the perturbation and  $\tilde{C}_1$  is a constant that depends on the vector field away from neighbourhoods of the equilibria on the RHC, and is therefore usually very difficult to calculate analytically.  $\tilde{C}_1$  will also depend on the precise form of the symmetry-breaking perturbations introduced and therefore we have been deliberately vague about the form of the perturbation: the logarithmic dependence  $T \propto \log(1/\gamma)$  appears to be very generally applicable.

One might therefore expect that, to a first approximation, the effect of the term  $\gamma(1-x)f(2\omega t)$  in (1) would be to replace the attracting RHC with an attracting periodic orbit whose period  $T \propto -\log \gamma$ . This is exactly what happens when the perturbation term does not explicitly depend on time, for example replacing  $\gamma(1-x)f(2\omega t)$  by  $\gamma(1-x)/2$  in (1), as illustrated in figure 1.

Since the logarithmic scaling of  $T$  with  $\gamma$  is well known, and since in this paper we will work in the regime in which  $\gamma$  is always small, the real interest lies in understanding how the presence of a second frequency  $2\omega$  (the factor of 2 is for consistency with the remainder of the paper), within the external forcing term, affects the dynamics. There is a clear distinction to be made between two cases:  $2\omega > 2\pi/T$  and  $2\omega < 2\pi/T$ . If the frequency of the external forcing  $2\omega$  is smaller than  $2\pi/T$  then we expect closed

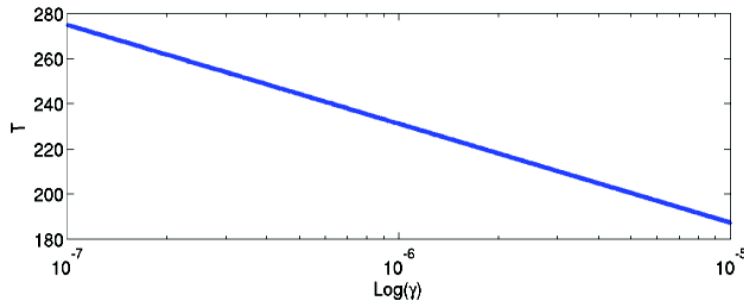


Figure 1: The period  $T$  of the periodic orbit generated by the time-independent perturbation term  $\gamma(1-x)/2$ , as a function of the perturbation amplitude  $\gamma$ . As expected, the relationship is very close to the form  $T = C_1 - \xi \log \gamma$ . The constant  $\xi \equiv (e^2 + ce + c^2)/e^3$  can be computed directly from the Poincaré map reduction. The constant  $C_1$  cannot easily be computed analytically. Other parameter values are  $c = 0.25$  and  $e = 0.2$ .

trajectories near the periodic orbit to make a number of excursions close to the full length of the (former) periodic orbit before closing. When the dynamics is investigated using Poincaré (return) maps, the corresponding orbit produces several discrete intersection points between the orbit and the hyperplane used in the construction of the return map. All these points lie on a single orbit of the continuous-time dynamics. In the case  $2\omega > 2\pi/T$  trajectories wind several times around a toroidal surface near the original periodic orbit before intersecting the hyperplane again. Thus closed orbits correspond to single points on the hyperplane and therefore to fixed points of a return map. A prominent feature of the dynamics that we explore are the existence of intervals in  $\omega$  over which closed orbits exist that are frequency-locked in the sense that the closed orbit winds  $k$  times around the toroidal surface before closing. The period  $T$  of such an orbit satisfies  $2\omega = 2\pi k/T$ .

### 2.3 The Poincaré map

The Poincaré (return) map method has become the standard approach for studying the dynamics near heteroclinic cycles and networks [21, 10], just as it is for the study of dynamics near periodic orbits. The idea of the method is to define a codimension-one hyperplane, (often called a ‘cross-section’), that all trajectories in a neighbourhood of the heteroclinic cycle intersect transversely. Repeated intersections define a return map from the cross-section to itself; studying the dynamics of this map enables us to understand the dynamics of trajectories near the periodic orbit or heteroclinic cycle. For a heteroclinic cycle we can make additional analytical progress by constructing the return map as the composition of two kinds of map: local maps within neighbourhoods of the saddle-type equilibrium points where the dynamics can be well approximated by the flow of the linearised equations (since the equilibrium points are hyperbolic), and global maps from one neighbourhood to another.

Previous work for example [19, 22, 23, 32, 33], uses the Poincaré map method to study the dynamics of an autonomous system containing a robust heteroclinic cycle. Only a few papers consider non-autonomous dynamics in any detail. Afraimovich et al. [2] derived a Poincaré return map for a system which is similar to the one we consider; section 5 discusses their results.

The derivation of the Poincaré map involves careful calculation of the local and global maps between cross-sections. Near equilibrium  $j$  on the RHC these are denoted  $H_j^{in}$  and  $H_j^{out}$  for  $j = 1, \dots, 3$ , as indicated on Figure 2. Because of the time-periodic perturbation, the local linearisations now include time-dependent terms. These time-dependent terms play a very important role in calculating the local map accurately. Our calculation also takes the time-periodicity of the global maps (diffeomorphisms between two cross sections) into account: numerically this can be seen to produce a better map than that

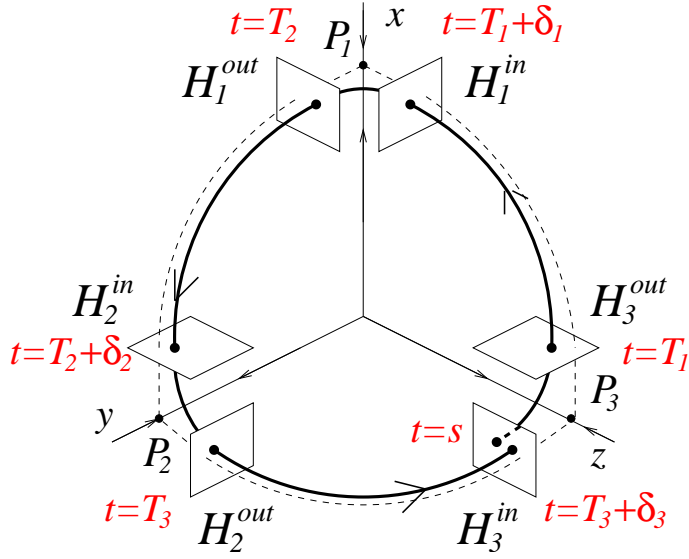


Figure 2: Sketch of the cross sections for the heteroclinic cycle and the times at which a trajectory near the cycle hits each cross section.

in [13], although the effect of the time-periodic terms is small since the time spent on these parts of the trajectory is much less than that spent near the equilibrium points.

As well as the values of the coordinates, the non-autonomous nature of the dynamics requires us to keep track of the elapsed time spent on each part of the trajectory. At leading order we obtain a return map that comprises a single coordinate and the elapsed time: it is a two-dimensional return map rather than the one-dimensional return maps that are usually obtained in the more common calculations for autonomous dynamics. Apart from this additional aspect, the detailed calculation of the Poincaré map is quite standard in nature: we leave the detail of the derivation and the explicit form of it to the Appendix. However, there are two points that deserve brief remarks here. Firstly, although the perturbation term only acts on the  $x$ -coordinate in our ODE system (1), the Poincaré map calculation is very similar for the more general case in which all three coordinates are perturbed, and the leading order result should be of the same form as (47). Secondly, the form of the Poincaré map at leading order in  $\gamma$  is unchanged if we replace the perturbation term  $\gamma(1-x)f(2\omega t)$  with  $\gamma f(2\omega t)$ . This is because the time-dependencies enter only through the local maps  $H_3^{in} \rightarrow H_3^{out}$  and  $H_2^{in} \rightarrow H_2^{out}$  at leading order. For these two local maps, however,  $x$  is  $O(\gamma)$  and so the  $\gamma x f(2\omega t)$  term is  $O(\gamma^2)$ .

For convenience when making detailed analysis and comparisons with numerical simulations of the ODEs, we will consider the system (1), setting  $f(2\omega t) = \sin^2(\omega t)$ , as [13]. As illustrated in Figure 2, we construct a return map  $F(x, t)$  from the cross section  $H_3^{in}$  (i.e. the plane  $\{y = h\}$  in a neighbourhood of  $P_3 = (0, 0, 1)$ ) to itself. The Poincaré map  $F(x, t)$  takes the form  $(\bar{x}, \bar{t}) = F(x, t) := (f_1(x, t), f_2(x, t))$ :

$$\begin{cases} f_1(x, t) = \mu x^d + \gamma [\mu_1 + \mu_2(-a_1 \cos(2\omega g) - b_1 \sin(2\omega g)) \\ \quad - \mu_4(-a_1 \cos(2\omega(\bar{t} - \delta_3)) - b_1 \sin(2\omega(\bar{t} - \delta_3))) \\ \quad - \mu_5(-a_2 \cos(2\omega \bar{t}) - b_2 \sin(2\omega \bar{t}))] + O(\gamma^2) \\ f_2(x, t) = t + \mu_3 - \xi \log(x) - \gamma \frac{\xi}{2e} [1 - a_2 \cos(2\omega t) + b_2 \sin(2\omega t)] x^{-1} + O(\gamma^2) \end{cases}, \quad (3)$$

where we define the coefficients  $a_1 = c^2/(c^2 + 4\omega^2)$ ,  $b_1 = 2c\omega/(c^2 + 4\omega^2)$ ,  $a_2 = e^2/(e^2 + 4\omega^2)$ ,  $b_2 = 2e\omega/(e^2 + 4\omega^2)$ ,  $\xi = (e^2 + ce + c^2)/e^3$ ,  $d = (c/e)^3$ , and the function  $g(x, t) := t + \mu_3 - \xi \log(x)$ . The coefficients  $\mu, \mu_1, \dots, \mu_5$  and  $\delta_3$  depend on the global maps and are not computable analytically. We make specific choices for these parameter values at various points in the analysis, to indicate that the dynamics of the ODEs are well captured by the dynamics of the above 2D map. In every case, the parameter values

that we give are the result of careful systematic scans through parameter space; however, the values are not the result of an optimisation procedure, so they are not ‘optimal’ in any precise sense. This is in line with our hope that the 2D map will elucidate the generic kinds of dynamics selected by the ODEs, and this is seen to be the case. We ignore terms in (3) that are  $O(\gamma^2)$  or higher: throughout the analysis of later sections we take  $\gamma$  sufficiently small in the analysis that these terms are certainly negligible.

In general in order to ensure that Poincaré maps such as  $F$  are well-defined, it is necessary to check that there exists an open set  $V$  in  $\mathbb{R}^2$  such that  $F(V) \subseteq V$ . In our case this is clear since each local and global map is a diffeomorphism defined on the intersections of open neighbourhoods of the points  $P_j$  with the relevant cross-sections and with the positive octant  $\mathbb{R}_+^3$ : there are no difficulties with cusp-shaped regions (or their complements) as often arise in the study of heteroclinic networks [19].

## 2.4 Asymptotic balances in different distinguished limits

In this subsection we motivate the existence of two distinct asymptotic regimes in the limit  $\gamma \ll 1$ : either  $\epsilon := d - 1$  is in addition small, so that  $\gamma^\epsilon \sim 1$  in the limit of small  $\gamma$ , or  $\epsilon$  is larger, so that  $\gamma^\epsilon \ll 1$  when  $\gamma \ll 1$ .

The dynamics of (3) depends in a complicated way on the relative size of the first term in  $f_1(x, t)$  compared to the remaining terms. We set the scene for the different cases that are considered in the next section by considering the dynamics of the one-dimensional map  $\bar{x} = l(x) := x^d + \gamma$ ; in some sense this is a ‘time-averaged’ and simplified version of  $\bar{x} = f_1(x, t)$  where, for simplicity and without loss of generality (after rescaling  $x$  and  $\gamma$ ), we can set  $\mu = \mu_1 = 1$ .

The first question we ask about the map  $l(x)$  concerns the existence of fixed points:  $l(\hat{x}) = \hat{x}$ . This depends on the relative sizes of the two small positive parameters  $\gamma$  and  $\epsilon := d - 1$ . When  $\epsilon > 0$  is small we are close to the resonant bifurcation at which (in the absence of the time-periodic forcing) the robust heteroclinic cycle would lose stability. We now estimate the region of the  $(\epsilon, \gamma)$  plane in which a fixed point  $\hat{x}$  exists. We note that since  $\epsilon > 0$  the graph of  $l(x)$  has zero gradient at  $x = 0$ , and the gradient is positive and monotonically increasing to  $+\infty$  in  $x > 0$ . We define  $x_m$  to be the point at which the gradient is unity:  $l'(x_m) = 1$ . We obtain, explicitly,

$$x_m = \left( \frac{1}{1 + \epsilon} \right)^{1/\epsilon}.$$

Now, since  $l(0) = \gamma > 0$ , if  $x_m \geq l(x_m)$ , i.e.  $\gamma \leq x_m - x_m^{1+\epsilon}$ , then necessarily the equation  $l(x) = x$  has at least one solution in  $x > 0$ . In other words, given  $\epsilon > 0$ , there exists

$$\gamma_1(\epsilon) := \left( \frac{1}{1 + \epsilon} \right)^{1/\epsilon} - \left( \frac{1}{1 + \epsilon} \right)^{(1+\epsilon)/\epsilon},$$

such that if  $\gamma \leq \gamma_1(\epsilon)$ , then  $l(x) = x$  has a solution. We denote the solution smaller than, or equal to,  $x_m$  by  $\hat{x}$  (i.e. this is the stable fixed point when two exist).

We now estimate the asymptotic size of  $\hat{x}$  in terms of  $\gamma$  and  $\epsilon$ . This is useful since it indicates under what conditions we may ignore the term  $x^d$  in (3) without qualitatively affecting the dynamics. Let  $p > 1$  be a constant. Then  $\hat{x} = \gamma^{1/p}$  is, directly, a solution of  $l(\hat{x}) = \hat{x}$  if and only if  $\epsilon = \epsilon_p(\gamma) := p \log(\gamma^{1/p} - \gamma) / \log \gamma - 1$ . Since  $\epsilon_p(\gamma)$  is a strictly monotonically increasing function of  $\gamma > 0$ , we may apply the inverse function theorem to assert that there exists a function  $\gamma_{2,p}(\epsilon)$  such that  $\hat{x} = \gamma^{1/p}$  if and only if  $\gamma = \gamma_{2,p}(\epsilon)$ , see Figure 3. We conclude that if  $(\epsilon, \gamma)$  lies in the region  $\Phi_p = \{(\epsilon, \gamma) : \gamma_{2,p}(\epsilon) \leq \gamma \leq \gamma_1(\epsilon)\}$ , then  $\gamma^{1/p} \leq \hat{x} \leq x_m$ . It follows that different choices of  $\epsilon$  and  $\gamma$  may lead to  $\hat{x}$  being either close to  $\gamma$  or  $\hat{x}$  being far larger than  $\gamma$ . This, in turn, implies that  $x^d$  can either be neglected or not, respectively, in (3).

Upper and lower bounds (denoted by  $B_1$  and  $B_2$ , respectively) on  $\hat{x}$  can be constructed by linear interpolation, using the monotonicity and convexity of  $l(x)$ , as shown in Figure 4. More precisely, consider the line  $L_1$  in the  $(x, l(x))$  plane joining the two points  $(0, \gamma)$  and  $(x_m, x_m^d + \gamma)$ .  $L_1$  intersects the diagonal

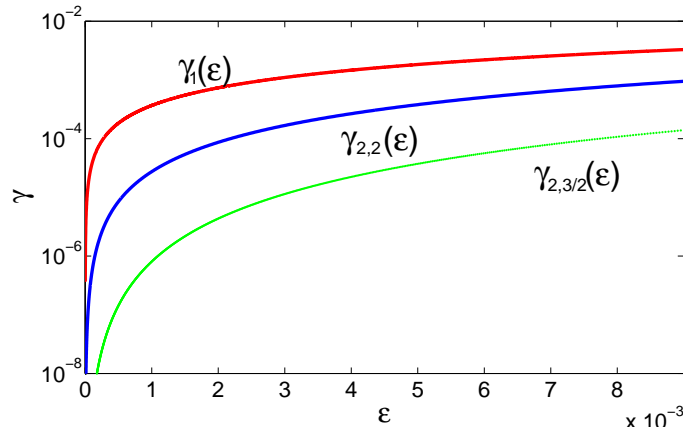


Figure 3: Log-linear plot of the  $(\epsilon, \gamma)$  plane illustrating the definition of the region  $\Phi_p$  which lies between the curves  $\gamma = \gamma_1(\epsilon)$  (upper curve, red) and  $\gamma = \gamma_{2,p}(\epsilon)$ , for any  $p > 1$ . For illustration we show two cases:  $p = 2$  (middle curve, blue) and  $p = 3/2$  (lowest curve, green).

at  $x = l(x) = \gamma x_m / (x_m - x_m^d)$ . Since  $l(x)$  is convex,  $L_1$  lies above  $l(x)$  for  $0 \leq x \leq x_m$ . In particular,  $L_1$  lies above the intersection point  $\hat{x}$  of  $l(x)$  with the diagonal. Hence it follows that we have the upper bound  $\hat{x} \leq B_1(\epsilon, \gamma) := \gamma x_m / (x_m - x_m^d)$ . Similarly, consider the line  $L_2$  defined as the line passing through  $(\gamma, \gamma^d + \gamma)$  and tangent to  $l(x)$  there. Since  $\gamma < \hat{x}$ , and the gradient of  $l(x)$  is increasing, the intersection of  $L_2$  and the diagonal, which occurs at  $B_2(\epsilon, \gamma) := \left(1 + \frac{\gamma^\epsilon}{1 - (1 + \epsilon)\gamma^\epsilon}\right) \gamma$ , is a lower bound for  $\hat{x}$ . To summarise:

$$B_2(\epsilon, \gamma) := \left(1 + \frac{\gamma^\epsilon}{1 - (1 + \epsilon)\gamma^\epsilon}\right) \gamma \leq \hat{x} \leq \frac{x_m}{x_m - x_m^d} \gamma =: B_1(\epsilon, \gamma).$$

Figure (4)(b) indicates these upper and lower bounds for  $\hat{x}$  in the case of  $e = 0.2$  and  $\gamma = 10^{-6}$ , varying  $c$  in order to vary  $\epsilon$  (recall that  $d := (c/e)^3$  and  $\epsilon := d - 1$ ). Further, since these scaling arguments are independent of the oscillating terms in the first equation of (3), we can use them to estimate the importance of the role of the  $x^d$  term when  $c$  is near  $e$ . For example, the  $x^d$  term can be ignored in the case  $c = 0.25$ ,  $e = 0.2$  for which  $\epsilon \equiv (c/e)^3 - 1 = 0.953125$ . This analysis justifies our procedure, when discussing the numerical simulations presented later, in which we typically fix  $e = 0.2$  and  $\gamma = 10^{-6}$  and consider the two contrasting cases  $c = 0.2001$  and  $c = 0.25$ .

In the following two sections we investigate the bifurcation structure of (simplified versions of) system (3) when varying the forcing frequency  $\omega$ , i.e. considering  $\epsilon$  and  $\gamma$  as fixed. Our discussion above can be summarised by saying either that we are in the case ‘ $\epsilon$  near 0’ meaning that, for a given  $\gamma$ ,  $\epsilon$  is small enough such that the term  $x^d$  must be included in the Poincaré map (3) since  $\gamma^\epsilon \sim 1$ . Or, in contrast, we will say that we are in the case ‘ $\epsilon$  of order unity’ if, for a given  $\gamma$ ,  $\epsilon$  is large enough that  $x^d$  can be ignored without causing qualitative changes to the bifurcation structure, i.e.  $\gamma^\epsilon \ll 1$ . The actual values of  $\epsilon$  that these situations correspond to will themselves depend on  $\gamma$ .

### 3 The weakly attracting regime: $\gamma, \epsilon \ll 1$ with $\gamma^\epsilon \sim 1$

Having worked carefully to construct the Poincaré map (3) in section 2.3, it is perhaps surprising that the dynamics of the map can be captured quantitatively by a much simpler form. In this section we justify this simpler form, and we then explore its behaviour in more detail, given that it is simple enough to be analytically tractable.

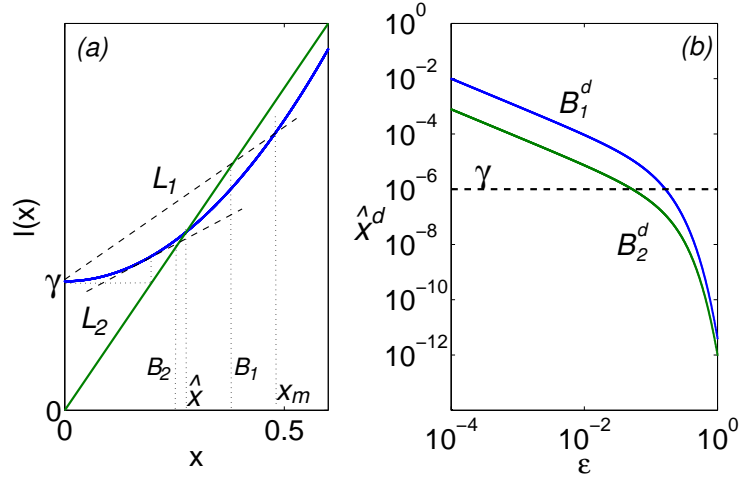


Figure 4: (a) The graph of  $l(x)$  (blue curve) illustrating the construction of the upper ( $B_1$ ) and lower ( $B_2$ ) bounds for  $\hat{x}$  at fixed  $\epsilon$  and  $\gamma$ , i.e.  $B_1(\epsilon, \gamma) < \hat{x} < B_2(\epsilon, \gamma)$ . The diagonal  $x = l(x)$  is shown in green. (b) The upper ( $B_1^d$ , blue) and lower ( $B_2^d$ , green) bounds for  $\hat{x}^d$  functions of  $\epsilon$  for  $e = 0.2$  and  $\gamma = 10^{-6}$ . (b) shows that when  $\epsilon \rightarrow 0$  at fixed positive  $\gamma$  we find that  $\hat{x}^d \gg \gamma$  while with increasing  $\epsilon$  at fixed  $\gamma$ ,  $\hat{x}^d$  rapidly becomes far smaller than  $\gamma$ .

The results of subsection 2.4 show that in the weakly attracting regime the term  $\mu x^d$  in  $f_1(x, t)$ , the first equation in (3), contributes to the leading-order determination of the size of fixed points  $\hat{x}$ . Moreover, when fixed points exist, assuming that the  $O(\gamma)$  terms in (3) do not vanish, we expect  $\hat{x} \gg \gamma$ . The precise form of the  $O(\gamma)$  terms in the first equation of (3) contributes (at fixed  $x$ ) a  $t$ -periodic function whose amplitude and phase depends on the forcing frequency  $\omega$ . The coefficients  $a_1$  and  $a_2$  are in fact close to each other in the weakly attracting regime, for all values of  $\omega$ , since the limit  $\epsilon \ll 1$  implies that the difference between  $c$  and  $e$  is small.

Given that the terms in the first equation in (3) contain several undetermined parameters ( $\mu_2, \mu_4, \mu_5$  and  $\delta_3$ ) that come from the global parts of the Poincaré return map, we propose replacing this complicated collection of quantitatively unknown terms with a single sinusoidal perturbation, i.e. we replace  $f_1(x, t)$  in (3) with

$$\bar{x} = \mu x^d + \gamma \mu_1 (1 + \sqrt{a_2} \sin(2\omega t)).$$

We turn now to the second equation of (3). The form of the  $O(\gamma)$  terms in  $f_2(x, t)$  can in fact be rewritten in a much simpler form using the new simplified form of  $f_1(x, t)$  above. This observation has its roots in the Taylor series argument, expanding in  $\gamma$ , that we used to derive (3). The  $O(\gamma)$  terms in the second equation of (3) arise naturally in a Taylor expansion of  $\log \bar{x}$ , so that we can collect the leading order and  $O(\gamma)$  terms together and write

$$\bar{t} = t + \mu_3 - \xi \log \bar{x},$$

as the most concise way to describe the  $t$ -dynamics, ignoring terms that are  $O(\gamma^2)$ . Note that the right hand side still contains non-trivial dependence on  $t$  since it contains  $\bar{x}$ , not  $x$ .

Putting these together, the simplified map  $(\bar{x}, \bar{t}) = F(x, t)$  takes the form

$$\begin{cases} \bar{x} &= \mu x^d + \gamma (1 + \sqrt{a_2} \sin(2\omega t)), \\ \bar{t} &= t + \mu_3 - \xi \log \bar{x}, \end{cases} \quad (4)$$

and for completeness we recall that  $a_2 = e^2/(e^2 + 4\omega^2)$ ,  $\xi = (e^2 + ce + c^2)/e^3$ ,  $d = (c/e)^3$ .  $\mu$  and  $\mu_3$  are parameters that arise from the global parts of the return map and hence may be adjusted to fit the ODE

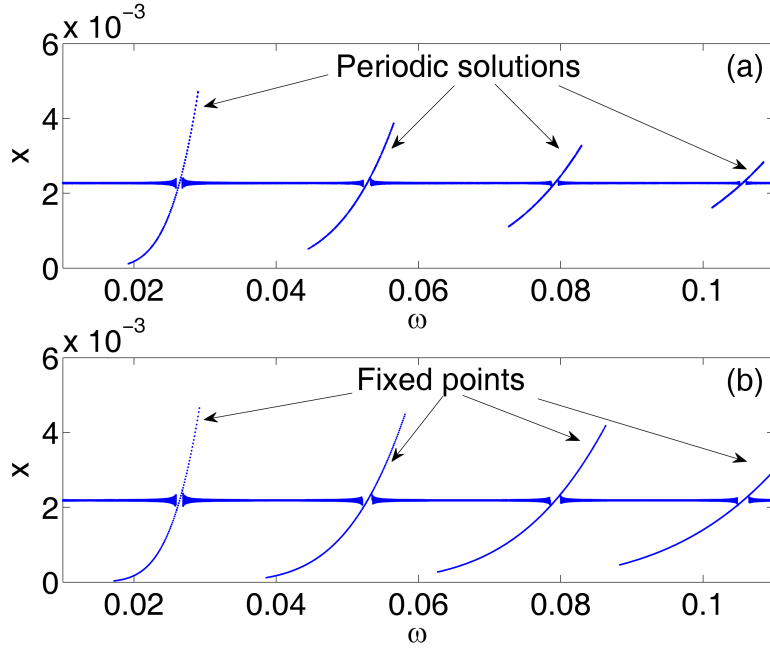


Figure 5: Comparison of the dynamics of the ODEs and the simplified model map (4). (a) Attractors for the dynamics of the ODE (1) for  $c = 0.2001$ ,  $e = 0.2$  and  $\gamma = 10^{-6}$ . We plot the  $x$ -coordinates of the points of two typical trajectories on the cross section  $H_3^{in}$  for each fixed  $\omega$  after transients have decayed. The curves in the figure correspond to frequency-locked periodic orbits in the ODEs. Bistability occurs in both ends of each curve. The horizontal ‘lines’ in the figure, which all sit near  $\hat{x} \approx 2.2 \times 10^{-3}$ , indicate (possibly complex) dynamics with  $|x - \hat{x}| = O(\gamma)$ . (b) Quantitatively similar dynamics observed by iterating the simplified model map (4) with parameters  $\gamma = 2 \times 10^{-5}$ ,  $\mu = 1$  and  $\mu_3 = 27$ . The four curved lines indicate the existence of fixed points for the return map; each curve exists over one of the first four frequency-locking intervals  $[\omega_k^-, \omega_k^+]$  for  $k = 1, \dots, 4$ , defined in section 3.1.

dynamics (we have taken  $\mu_1 = 1$  since, numerically, this appears to be a reasonable value, and variation in  $\mu_1$  corresponds only to a rescaling of  $\gamma$ ).

Figure 5 compares bifurcation diagrams computed numerically via integration of the ODE system and from iteration of the 2D model map (4), using  $\omega$  as the bifurcation parameter, in the case  $c = 0.2001$ ,  $e = 0.2$  (and so  $\epsilon \approx 0.0015$ ) and  $\gamma = 10^{-6}$ . Although the end points of the frequency-locking intervals are not quite at the same values of  $\omega$ , it is clear that many other aspects are captured extremely accurately and the main global features of the dynamics in these two systems are essentially identical. Thus the numerical results confirm our intuition in replacing the complicated parts of  $f_1(x, t)$  by a much simpler sinusoidal term.

We observe that, in the map, orbits are attracted either to an invariant curve or to a fixed point, and indeed both may be stable simultaneously, see figure 7 for an example that will be discussed in detail presently. The corresponding dynamics for the ODE system is the existence of a stable invariant torus or periodic orbit which again may both be stable at the same time. Moreover, these attractors alternate in a regular pattern as  $\omega$  increases.

Frequency-locked periodic orbits occur in intervals on  $\omega$  which can be identified by considering a plot of the return period  $T = \bar{t} - t$  against  $\omega$ . Such a periodic orbit must have a period that is an integer multiple of the forcing frequency  $\pi/\omega$ , i.e. a period  $T = k\pi/\omega$ , for some  $k \in \mathbb{N}$ . The curves in Figure 6 therefore lie on the hyperbolas  $T(\omega) = k\pi/\omega$  indexed by  $k$ .

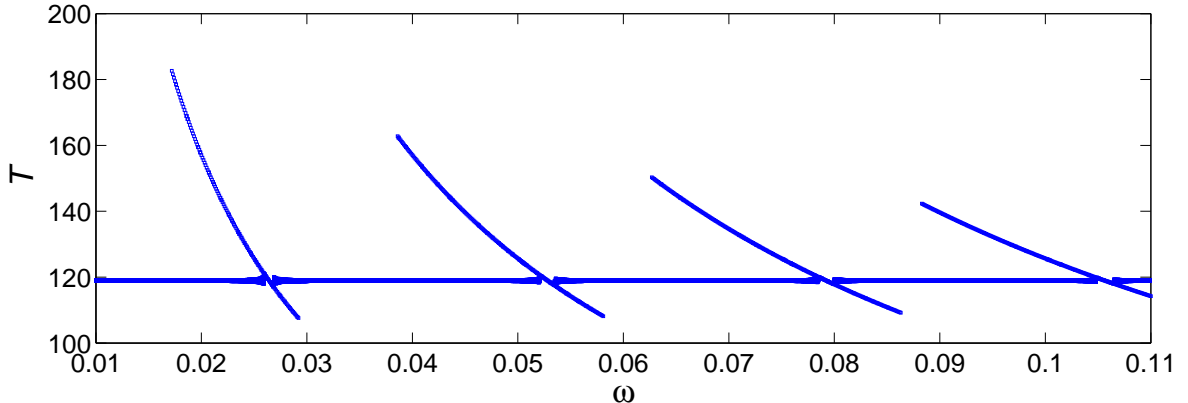


Figure 6: The  $\omega$ - $T$  plot for the system (4) for  $c = 0.2001$ ,  $e = 0.2$ ,  $\mu = 1$ ,  $\mu_3 = 27$  and  $\gamma = 2 \times 10^{-5}$ . The curves, on which frequency-locked periodic orbits exist (compared to figure 5), are sections of hyperbolas as discussed in the text, i.e.  $T = k\pi/\omega$  for integers  $k = 1, \dots, 4$ .

In the remainder of this section, we will consider (4) as a model to enable us to understand the dynamics of the ODEs (1) in the case  $\epsilon$  near 0. We give a detailed analysis near the ends and near the centre of the frequency locking intervals for small  $\omega$  in subsections 3.1 and 3.2 respectively. In subsection 3.3 we show that for sufficiently small frequencies  $\omega$ , below  $\omega_1^-$ , there exists a globally attracting invariant curve within the 2D map. In the case  $\omega \rightarrow \infty$ , the dynamics are the same as in the case  $\omega \rightarrow \infty$  for  $\epsilon$  large: this case is studied in section 4.1.

### 3.1 Local bifurcations

In this section we discuss the bifurcations that occur at the end of the frequency locking intervals in the model system.

Consider varying  $\omega$  through the  $k^{\text{th}}$  frequency locking interval which we denote by  $\omega_k^- \leq \omega \leq \omega_k^+$  and define below. A fixed point  $(x, t) = (x(\omega), t(\omega))$  in the system (4) exists, for a given  $\omega$ , if and only if

$$\begin{cases} x &= \mu x^d + \gamma(1 + \sqrt{a_2} \sin(2\omega t)) \\ \mu_3 - \xi \log x &= k\pi/\omega \end{cases}, \quad (5)$$

hence  $x(\omega) = \exp((\mu_3 - k\pi/\omega)/\xi)$ . Since  $x(\omega)$  is monotonically increasing, tends to zero as  $\omega \rightarrow 0$  and tends to  $e^{\mu_3/\xi}$  as  $\omega \rightarrow \infty$ , which is much larger than the typical values of  $x$  that we are interested in for our choices of parameters, we define  $\omega_k^-$  to be the smallest  $\omega$  such that  $x(\omega)$  satisfies the first equation of (5) for some  $t$ . At  $\omega = \omega_k^-$ ,  $\sin(2\omega t)$  takes the value  $-1$  and so  $t(\omega_k^-) = \frac{3\pi}{4\omega_k^-}$ .

For  $\omega$  is slightly above  $\omega_k^-$ ,  $x(\omega) > x(\omega_k^-)$  and there exist two values for  $t(\omega)$ , one larger and one smaller than  $t(\omega_k^-)$ , such that  $(x(\omega), t(\omega))$  satisfy (5). The stability of these fixed points can be easily computed. The Jacobian of system (4) is

$$\begin{pmatrix} d\mu x^{d-1} & 2\omega\sqrt{a_2} \cos(2\omega t)\gamma \\ -(\xi/\bar{x})d\mu x^{d-1} & 1 - (\xi/\bar{x})2\omega\sqrt{a_2} \cos(2\omega t)\gamma \end{pmatrix}.$$

When  $\omega = \omega_k^-$ , the two eigenvalues are  $\lambda_1 = 1$  and  $\lambda_2 = d\mu x^{d-1}$  which is less than unity in magnitude. For  $\omega$  slightly above  $\omega_k^-$ ,  $\lambda_1$  is less than unity if  $t(\omega) > t(\omega_k^-)$  and greater than unity otherwise, while  $\lambda_2$  is positive and less than unity if  $\omega$  is close enough to  $\omega_k^-$ . Accordingly, we have proved the following proposition.

**Proposition 3.1** *System (4) undergoes a saddle-node bifurcation at  $\omega = \omega_k^-$  and a stable fixed point  $(x(\omega), t(\omega))$  exists in  $\omega > \omega_k^-$  for  $|\omega - \omega_k^-|$  sufficiently small.*

A similar argument applies to the right-hand end  $\omega = \omega_k^+$  of the  $k^{\text{th}}$  frequency-locking interval where another saddle-node bifurcation occurs and the stable and unstable fixed points disappear. These saddle-node bifurcations correspond to the ends of the segments of curves shown in Figures 5 and 6.

From Figure 5, it appears that there exists a separate attracting invariant set near  $x = 0.0022$ . Since  $x(\omega)$  crosses this value as  $\omega$  increases for each fixed  $k$ , the question arises as to how the dynamics of the system change when the stable fixed point  $(x(\omega), t(\omega))$  passes near the invariant set. We analyse this situation in the next section.

### 3.2 Global bifurcations of the system

We now turn to investigating the dynamics near the centre of the  $k^{\text{th}}$  frequency-locking window. As shown in Figure 7, the stable fixed point  $(x(\omega), t(\omega))$  moves from below to above the other attracting invariant set when  $\omega$  increases. This transition is mediated by global bifurcations, and in fact we show, at least asymptotically, that the bifurcation structure is that of the well-known forced damped pendulum.

Let  $(\hat{x}, \omega_k)$  be values of  $x$  and  $\omega$  at the centre of the  $k^{\text{th}}$  frequency-locking interval, i.e. we define them to satisfy

$$\begin{cases} \hat{x} &= \mu \hat{x}^d + \gamma \\ \mu_3 - \xi \log \hat{x} &= \frac{k\pi}{\omega_k} \end{cases}.$$

Since we are working in the limit  $\epsilon \ll 1$ , we may approximate  $\xi = \frac{1}{e}(1 + c/e + c^2/e^2) \approx 3/e$ . Now consider values of  $(x, \omega)$  near  $(\hat{x}, \omega_k)$ . We define the new variables  $(y, \lambda)$  as follows. Let  $x_n = \hat{x}(1 + y_n)$  and  $\mu_3\omega - (3\omega/e)\log \hat{x} = k\pi + (3\omega/e)\lambda$ ; we consider  $|y|$  and  $|\lambda|$  to be small. We also define  $s_n = 2\omega t_n$  and substitute all these into (4). We obtain

$$\begin{aligned} x_{n+1} = \hat{x}(1 + y_{n+1}) &= \mu \hat{x}^d(1 + y_n)^d + \gamma(1 + \sqrt{a_2} \sin s_n), \\ &= (\hat{x} - \gamma)(1 + dy_n + O(y_n^2)) + \gamma(1 + \sqrt{a_2} \sin s_n), \\ &= (\hat{x} - \gamma)(1 + y_n) + (\hat{x} - \gamma)(\epsilon y_n + O(y_n^2)) + \gamma(1 + \sqrt{a_2} \sin s_n). \end{aligned}$$

Dropping  $O(y_n^2)$  and  $O(\epsilon y)$  terms we obtain

$$y_{n+1} - y_n = \hat{x}^{-1}\gamma(-y_n + \sqrt{a_2} \sin s_n).$$

For the time coordinate, using (4) we obtain

$$\begin{aligned} 2\omega(\bar{t} - t) \equiv s_{n+1} - s_n &= 2\omega\mu_3 - \frac{6\omega}{e}(\log \hat{x} + \log(1 + y_{n+1})), \\ &= 2\omega\mu_3 - \frac{6\omega}{e}(\log \hat{x} + y_{n+1}) + O(y_{n+1}^2) \\ &\approx \frac{6\omega}{e}\lambda - \frac{6\omega}{e}y_{n+1}. \end{aligned}$$

Therefore,

$$\begin{aligned} \frac{y_{n+1} - y_n}{\hat{x}^{-1}\gamma} &= -y_n + \sqrt{a_2} \sin s_n, \\ \frac{s_{n+1} - s_n}{\hat{x}^{-1}\gamma} &= \frac{6\omega}{\hat{x}^{-1}\gamma e}(\lambda - y_{n+1}). \end{aligned}$$

Since  $\gamma^{1/p} \leq \hat{x} \leq x_m$  for some fixed  $p > 1$ , we have  $\hat{x}^{-1}\gamma \rightarrow 0$  if  $(\epsilon, \gamma) \rightarrow 0$  within  $\Phi_p$  (see section 2.4). Hence, these difference equations are well approximated by the differential equations

$$\begin{cases} \dot{y} &= -y + \sqrt{a_2} \sin s, \\ \dot{s} &= \eta^2(\lambda - y), \end{cases} \quad (6)$$

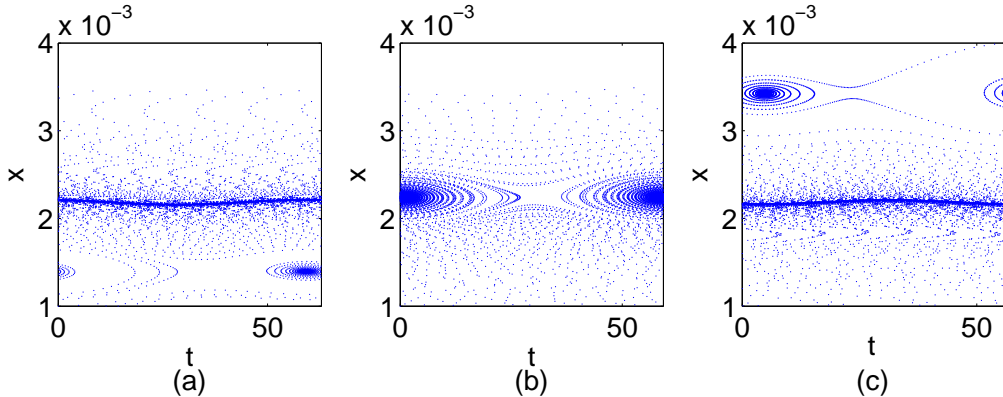


Figure 7: Iterates of the 2D map (4) from many initial conditions at (a)  $\omega = 0.05$ , (b)  $\omega = 0.053$  and (c)  $\omega = 0.056$ . Parameters are  $c = 0.2001$ ,  $e = 0.2$ ,  $\mu_3 = 27$  and  $\gamma = 2 \times 10^{-5}$ . (a) and (c) show that a stable fixed point exists alongside the invariant curve. As  $\omega$  increases, the stable fixed point moves from below to above the invariant curve. The dynamics in parts (a), (b) and (c) of this figure correspond to the sketches in figure 8 parts (b), (d) and (f) respectively.

where  $\eta^2 = 6\omega/(\hat{x}^{-1}\gamma e)$  is a parameter that we formally require to remain  $O(1)$  in the limit. Strictly speaking, this would demand varying  $k$  as we take  $\gamma$  and  $\epsilon$  smaller; for fixed  $k$  we find that  $\eta$  increases, albeit slowly, as  $\gamma \rightarrow 0$ . This increase in  $\eta$  can be estimated asymptotically as follows. As  $\hat{x} \rightarrow 0$ , for any fixed  $k$ , we find  $\omega_k \rightarrow 0$ , indeed  $\omega_k \sim -ek\pi/(3 \log \hat{x})$ . Suppose that  $\hat{x} = \gamma^{1/p}$  for some  $p > 1$ . Then

$$\eta^2 \sim -\frac{2pk\pi}{\gamma^{(p-1)/p} \log \gamma}, \quad (7)$$

which increases without bound as  $\gamma \rightarrow 0$  for any fixed  $p > 1$ . For the values of  $\epsilon$  and  $\gamma$  that we have investigated numerically the agreement between the dynamics of the differential equations and the 2D map remains good over a range of  $k$ . By way of illustration, Figure 9 shows that the ODE system (6) possesses very similar dynamics to the map system (4) near  $\omega_k$  for  $k = 2$ . Here, we compute  $\omega_k = 0.053$  and  $\hat{x} = 2.2 \cdot 10^{-3}$ , using the parameters  $c = 0.2001$ ,  $e = 0.2$ ,  $\mu_3 = 27$  and  $\gamma = 2 \times 10^{-5}$ .

Combining the two equations in (6), we obtain

$$\begin{aligned} \ddot{s} &= -\eta^2 \dot{y} = \eta^2 y - \eta^2 \sqrt{a_2} \sin s, \\ &= -\dot{s} + \eta^2 \lambda - \eta^2 \sqrt{a_2} \sin s. \end{aligned}$$

After rescaling time derivatives by  $d/dt \rightarrow \eta d/dt$  we obtain the canonical equation for a damped pendulum with a constant applied torque:

$$\ddot{s} + \eta^{-1} \dot{s} + \sqrt{a_2} \sin s = \lambda. \quad (8)$$

Physically, for the pendulum, the  $\eta^{-1} \dot{s}$  term corresponds to linear friction: oscillations are strongly damped when  $\eta$  is small. The  $\lambda$  term corresponds to the constant applied torque. The dynamics of equation (8) are quite simple and have been fully investigated ([11, 5]). If  $|\sqrt{a_2}^{-1} \lambda| > 1$  then the only invariant set is a stable periodic orbit. If  $|\sqrt{a_2}^{-1} \lambda| < 1$  and  $\eta^{-1}$  is large then only equilibria exist. However, bistability occurs when  $|\sqrt{a_2}^{-1} \lambda| < 1$  and  $\eta^{-1}$  is small. In this case, the stable equilibrium and periodic orbit coexist. Figure 10 shows the schematic bifurcation diagram for (8).

To summarise, this analysis indicates that the 2D map (4) can be well approximated by the ODE (8) in the case  $\epsilon$  near zero, i.e. within the distinguished limit  $\epsilon \rightarrow 0$ ,  $\gamma \rightarrow 0$  such that  $\hat{x}^{-1} \gamma \rightarrow 0$  as discussed in section 2.4, and in which  $\eta$  remains  $O(1)$ . Within this asymptotic limit we would expect the bistable case in which we have coexistence of a stable equilibrium and a stable periodic orbit to arise for  $\eta$  sufficiently

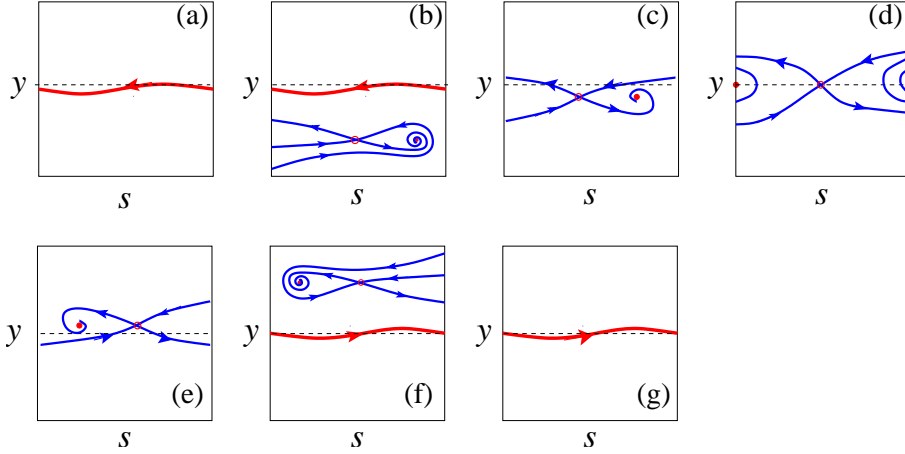


Figure 8: Sketch phase portraits in the  $(s, y)$  plane for the system (6) corresponding to the cases  $\lambda < 0$ : (a), (b) and (c);  $\lambda = 0$ : (d); and  $\lambda > 0$ : (e), (f) and (g). Red dots denote fixed points: one stable (filled circle) and one unstable (unfilled circle). The thin dashed line denotes  $y = 0$ . The one-dimensional invariant curve exists in (a), (b), (f) and (g) near  $y = 0$  and is coloured red. The blue curves are the stable and unstable manifolds of the unstable fixed point. As  $\omega$  increases, i.e.  $\lambda$  moves from negative to positive, a pair of fixed points appears via a saddle-node bifurcation: (a) $\rightarrow$ (b); the system then undergoes a global bifurcation (shown in (c)) when the invariant curve disappears; the fixed points then move from below to above the line  $y = 0$ : (c),(d) and (e); a second global bifurcation takes place (shown in (e)) and the invariant curve reappears; the pair of fixed points then disappears again via a second saddle-node bifurcation: (f) $\rightarrow$ (g).

large, therefore this case dominates at small  $\epsilon$ . At larger  $\epsilon$ ,  $\eta$  decreases and we move out of the bistable case. These observations agree with the numerical results shown in figures 5 and 15 here, and also with figures 2 and 3 in [13].

Therefore, we have proved the following proposition:

**Proposition 3.2** *The dynamics of the system (4) are asymptotically equivalent to the dynamics of a damped pendulum with constant torque (8) near the centres of each of the frequency-locking intervals  $[\omega_k^-, \omega_k^+]$  when the parameters  $\epsilon$  and  $\gamma$  are both sufficiently small as long as  $(\epsilon, \gamma) \in \Phi_p$  for some  $p > 1$ .*

### 3.3 The dynamics for $\omega < \omega_1^-$

For any fixed  $\epsilon$  and  $\gamma$  there exists a minimum frequency  $\omega$  at which frequency locking is possible: this is the left-hand end of the first interval, denoted  $\omega_1^-$  above. In this subsection we investigate the dynamics for forcing frequencies smaller than this:  $0 \leq \omega < \omega_1^-$ . We are able to prove that if  $\omega$  is sufficiently small then the maximal attractor for the dynamics is an invariant curve. This ensures, for example, that the bistable dynamics of the previous subsection cannot occur.

We first prove a theorem analogous to that proved by Afraimovich, Hsu and Lin [2] (and stated here as Theorem 5.1) which provides a sufficient condition for the existence of an invariant curve as the maximal attractor for their map, which took the form (20).

Consider the following system  $(\bar{x}, \bar{\theta}) = F(x, \theta)$  defined by:

$$\begin{cases} \bar{x} &= \mu x^d + \gamma(1 + a \sin \theta), \\ \bar{\theta} &= \theta + \tilde{\omega} - \tilde{\eta} \log \bar{x}. \end{cases} \quad (9)$$

Fix  $\gamma$  and (without loss of generality) set  $\mu = 1$ . Recall from section 2.4 that  $\hat{x}$  satisfies the equation  $\hat{x} = \hat{x}^d + \gamma$  and suppose  $\hat{x}$  is of order  $\gamma^{1/p}$  for some  $p > 1$ , so that  $\hat{x} \gg \gamma$ ; this can be done by letting  $d$

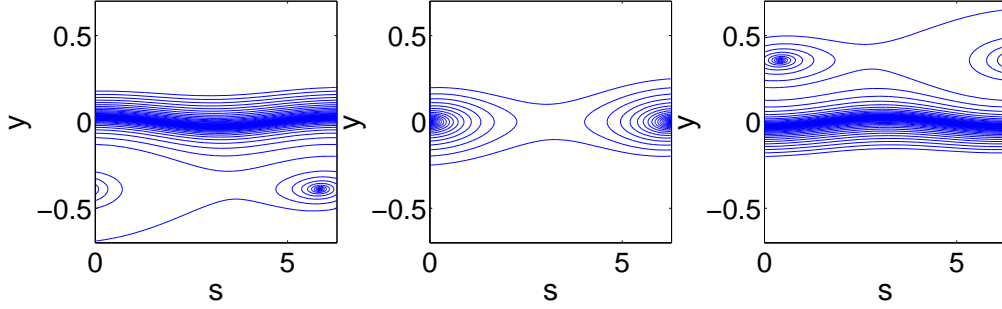


Figure 9: The dynamics of the system (6) at (a)  $\omega = 0.05$  ( $\lambda = -0.3725$ ), (b)  $\omega = 0.053$  ( $\lambda = 0$ ) and (c)  $\omega = 0.056$  ( $\lambda = 0.3725$ ). Parameters are  $c = 0.2001$ ,  $e = 0.2$ ,  $\mu_3 = 27$  and  $\gamma = 2 \times 10^{-5}$ . We take  $\omega_k = 0.053$  and  $\hat{x} = 2.2 \times 10^{-3}$ . The curves are trajectories from three initial conditions.

be close enough to 1. Let  $A = 2a/(1 - d\hat{x}^{d-1})$ . We begin by proving that

$$D = \{(x, \theta) : 0 < \hat{x} - A\gamma \leq x \leq \hat{x} + A\gamma, 0 \leq \theta \leq 2\pi\}, \quad (10)$$

is an invariant region for  $F$ .

**Lemma 3.1** *The annular region  $D \subset \mathbb{R} \times S^1$  is forward-invariant under iteration of the map  $F$ .*

**Proof:** Suppose that  $(x, \theta) \in D$ , so that in particular  $x < \hat{x} + A\gamma$ , then by substituting for  $\hat{x}$  and Taylor expanding we obtain

$$\begin{aligned} \bar{x} &\leq (\hat{x} + A\gamma)^d + \gamma(1 + a \sin \theta) = \hat{x}^d + A\gamma d\hat{x}^{d-1} + \gamma + \gamma a \sin \theta + O(\gamma^2), \\ &\leq \hat{x} + A\gamma d\hat{x}^{d-1} + \gamma a \sin \theta + O(\gamma^2), \\ &\leq \hat{x} + \gamma(Ad\hat{x}^{d-1} + a) + O(\gamma^2) = \hat{x} + \gamma(a - ad\hat{x}^{d-1} + 2ad\hat{x}^{d-1}) / (1 - d\hat{x}^{d-1}) + O(\gamma^2), \\ &\leq \hat{x} + \gamma(a + ad\hat{x}^{d-1}) / (1 - d\hat{x}^{d-1}) + O(\gamma^2) < \hat{x} + A\gamma + O(\gamma^2), \end{aligned}$$

since  $d\hat{x}^{d-1} < dx_m^{d-1} = 1$  by the definition of  $x_m$  in section 2.4. Similarly,  $\hat{x} - A\gamma$  provides a lower bound for  $\bar{x}$  of  $F$  in  $D$  since

$$\begin{aligned} \bar{x} &\geq (\hat{x} - A\gamma)^d + \gamma(1 + a \sin \theta) = \hat{x}^d - \gamma d\mu\hat{x}^{d-1}A + \gamma + \gamma a \sin \theta + O(\gamma^2), \\ &\geq \hat{x} - \gamma d\hat{x}^{d-1}A + \gamma a \sin \theta + O(\gamma^2), \\ &\geq \hat{x} - \gamma(d\hat{x}^{d-1}A + a) + O(\gamma^2) = \hat{x} - \gamma(a + ad\hat{x}^{d-1}) / (1 - d\hat{x}^{d-1}) + O(\gamma^2) > \hat{x} - A\gamma + O(\gamma^2). \end{aligned}$$

Hence  $D$  is a forward-invariant region for the map  $F$ .  $\square$

This lemma implies the existence of an attractor for  $F$  in  $D$ . However, we cannot at the moment identify what it looks like. The ‘Annulus Principle’ provides sufficient conditions for  $F$  to possess an invariant closed curve as its maximal attractor. We define the maximal attractor of  $F$  in  $D$  to be  $\bigcap_{n=1}^{\infty} F^n(D)$ .

**Theorem 3.1** (*‘Annulus Principle’ [1]*) *Let  $\Psi : (x, \theta) \mapsto (\bar{x}, \bar{\theta})$ ,  $x \in \mathbb{R}^k$ ,  $\theta \in \mathbb{T}^\ell$ , be a map of the form*

$$\bar{x} = f(x, \theta), \quad \bar{\theta} = \theta + g(x, \theta) \pmod{2\pi},$$

where  $f, g$  are differentiable functions which are  $2\pi$ -periodic in  $\theta = (\theta_1, \dots, \theta_\ell)$ . Assume that  $\Psi$  maps an annulus  $D = \{(x, \theta) : |x| \leq r_0\}$ , for some  $r_0 > 0$ , into its interior. Define the norm for vectors or

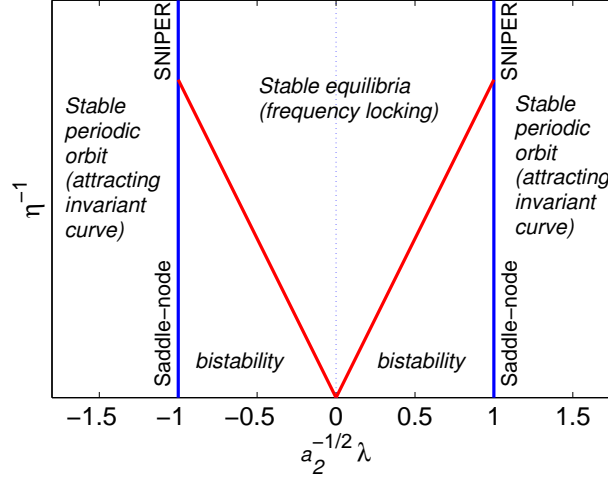


Figure 10: Bifurcation diagram for the forced pendulum with torque (8) which is equivalent to the Poincaré map (4) for small  $\epsilon$ .  $\omega_k$  denotes the centre of the  $k^{\text{th}}$  frequency-locking interval in  $\omega$  and  $\lambda \propto \omega - \omega_k$ . Saddle-node bifurcations occur on the vertical (blue) lines at  $\lambda^2 = a_2$  below the codimension-two points where they meet the diagonal (red) global bifurcation lines. SNIPER bifurcations occur at  $\lambda^2 = a_2$  above these points.

matrices in  $D$ :  $\|\cdot\| = \sup_{(x,\theta) \in D} |\cdot|$ , where  $|\cdot|$  is the relevant Euclidean norm. If

- (a)  $\|(I + g_\theta)^{-1}\| < \infty$ ,
- (b)  $\|f_x\| < 1$ ,
- (c)  $1 - \|(I + g_\theta)^{-1}\| \cdot \|f_x\| > 2\sqrt{\|(I + g_\theta)^{-1}\|^2 \cdot \|g_x\| \cdot \|f_\theta\|}$ ,
- (d)  $1 + \|(I + g_\theta)^{-1}\| \cdot \|f_x\| < 2\|(I + g_\theta)^{-1}\|$ ,

where  $I$  is the  $\ell \times \ell$  identity matrix and subscripts indicate differentiation with respect to the corresponding variables, then the maximal attractor in  $D$  is an invariant  $M$ -dimensional torus which is the graph of a smooth function  $x = h(\theta)$ .

We use the Annulus Principle to prove the following theorem concerning the dynamics of (9), setting  $\mu = 1$  without loss of generality.

**Theorem 3.2** *Suppose  $d$  and  $\gamma$  take values so that  $\hat{x} \gg \gamma$ . Then there exists a constant  $\delta$ , depending on  $d$  and  $\gamma$ , such that if  $\tilde{\eta}a < \delta$  and  $a < \frac{(x_m - \hat{x})(1 - d\hat{x}^{d-1})}{2\gamma}$ , then there exists an invariant closed curve as the maximal attractor for  $F$  in  $D$ .*

Recall that (in section 2.4)  $x_m$  is defined by the relation  $d\mu x_m^{d-1} = 1$ .

**Proof:** Referring to (9) we set  $f(x, \theta) = x^d + \gamma(1 + a \sin \theta)$ ,  $g(x, \theta) = \tilde{\omega} - \tilde{\eta} \log \bar{x}$ ,  $M = \hat{x} + 2a\gamma / (1 - d\hat{x}^{d-1}) \equiv \hat{x} + A\gamma$  and  $m = \hat{x} - 2a\gamma / (1 - d\hat{x}^{d-1}) \equiv \hat{x} - A\gamma$ . Note that if  $a < (x_m - \hat{x})(1 - d\hat{x}^{d-1}) / (2\gamma)$  then it follows immediately that  $M < x_m$ .

Let  $(x, \theta) \in D$ . We proceed to check each of the conditions (a)-(d) in turn.

(a) We compute that

$$|g_\theta| = \left| -\frac{\gamma \tilde{\eta} a \cos \theta}{x^d + \gamma(1 + a \sin \theta)} \right|.$$

It is easy to prove that for each fixed  $x$ , the maximal value of the right hand side in this last equality when varying  $\theta$  is

$$\frac{\tilde{\eta}a\gamma}{\sqrt{(\mu x^d + r)^2 - a^2\gamma^2}},$$

which is certainly less than 1 for  $\tilde{\eta}a$  small enough. In this case,

$$\|(I + g_\theta)^{-1}\| = \left(1 - \frac{\gamma\tilde{\eta}a}{\sqrt{(m^d + \gamma)^2 - a^2\gamma^2}}\right)^{-1} < \infty$$

always holds, and moreover  $\|(I + g_\theta)^{-1}\| \rightarrow 1$  as  $\tilde{\eta}a \rightarrow 0$ .

(b) We compute that  $\|f_x\| = \|dx^{d-1}\| \leq dM^{d-1} < dx_m^{d-1} = 1$  since  $\hat{x}$  is smaller than  $x_m$  and  $dx_m^{d-1} = 1$  by the definition of  $\hat{x}$  and  $x_m$  in section 2.4.

(c) We compute that

$$\|g_x\| = \left\| \tilde{\eta} \frac{dx^{d-1}}{x^d + \gamma(1 + a \sin \theta)} \right\| < \tilde{\eta} \frac{dM^{d-1}}{m},$$

since  $x^d + \gamma(1 + a \sin \theta) > m$  by Lemma 3.1. We observe also that  $\|f_\theta\| \leq a\gamma$ . By letting  $\tilde{\eta}a \rightarrow 0$ ,  $\|(I + g_\theta)^{-1}\|$  will tend to 1 and  $\|g_x\| \|f_\theta\|$  will tend to 0. Thus the third condition for the ‘Annulus Principle’ holds.

(d) Since  $\|(I + g_\theta)^{-1}\|(2 - \|f_x\|) \rightarrow 2 - \|f_x\|$ , which is greater than unity, as  $\tilde{\eta}a \rightarrow 0$ , the fourth condition also holds.

Hence, the conditions of Theorem 3.1 are met as long as  $\tilde{\eta}a$  sufficiently small, and so the result is proved.  $\square$

In our case, referring back to (4), we have  $\theta = 2\omega t$ ,  $a = \sqrt{a_2} = e/\sqrt{e^2 + 4\omega^2}$  and  $\tilde{\eta} = 2\omega\xi = 2\omega(e^2 + ce + c^2)/e^3$ . Note that the definition of the invariant set  $D$  in (10) depends implicitly on  $\omega$  through  $a$ , however since  $\sqrt{a_2} \nearrow 1$  as  $\omega \searrow 0$ , we can obtain an invariant set  $D_0$  which is independent of  $\omega$  by replacing  $a$  by unity in the definition of  $A$  before equation (10). Then, because  $\tilde{\eta}a = 2\omega\xi\sqrt{a_2}$  tends to 0 as  $\omega \rightarrow 0$ , we have the corollary below.

**Corollary 3.1** *Suppose  $d$  and  $\gamma$  are such that  $\hat{x} \gg \gamma$ . Then there exists an  $\omega_0$ , depending on  $d$  and  $\gamma$ , such that for all  $\omega < \omega_0$ , the system of equations (4) has an invariant closed curve as its maximal attractor in  $D_0$ .*

## 4 The strongly attracting regime: $\gamma \ll 1$ with $\gamma^\epsilon \ll 1$

In this section we consider the dynamics of (3) when  $d$  is not asymptotically close to unity, equivalently  $\epsilon := d - 1$  is not small, so that  $\gamma^\epsilon \ll 1$ . By the results in section 2.4, in this case the  $x^d$  term in the first equation of (3) is asymptotically smaller than the other terms which are  $O(\gamma)$ , and in the absence of perturbation (i.e.  $\gamma = 0$ ) the RHC is strongly attracting. Therefore the Poincaré map (3) can be approximated by dropping the  $x^d$  term to give

$$\begin{cases} \bar{x} = f_1(x, t) = \gamma [\mu_1 + \mu_2(-a_1 \cos(2\omega g) - b_1 \sin(2\omega g)) \\ \quad - \mu_4(-a_1 \cos(2\omega(\bar{t} - \delta_3)) - b_1 \sin(2\omega(\bar{t} - \delta_3))) \\ \quad - \mu_5(-a_2 \cos(2\omega \bar{t}) - b_2 \sin(2\omega \bar{t}))], \\ \bar{t} = f_2(x, t) = g - \gamma\xi/(2e)[1 - a_2 \cos(2\omega t) + b_2 \sin(2\omega t)]x^{-1}, \end{cases} \quad (11)$$

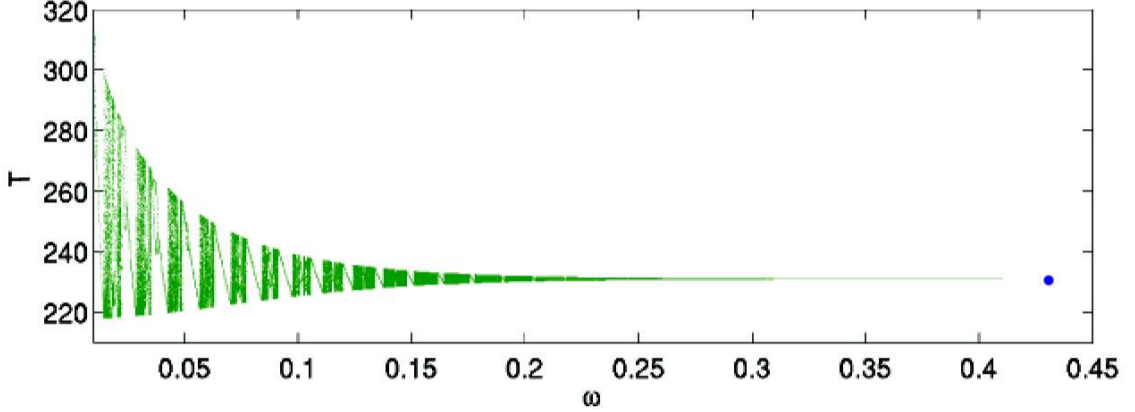


Figure 11: The dynamics of the ODEs (1) as  $\omega \rightarrow \infty$ , for  $\gamma = 10^{-6}$ . The range of return times  $T$  for trajectories reduces as  $\omega$  increases, tending, as  $\omega \rightarrow \infty$ , to the return time expected for the RHC subjected only to the time-averaged perturbation; this value is indicated by the blue dot at  $\omega \approx 0.43$  and agrees with figure 1.

where  $g = t + \mu_3 - \xi \log x$ .

This system turns out to be a little more complicated than (4) which was considered in the previous section. To begin with we consider with two asymptotic cases:  $\omega \gg 1$  (section 4.1) and  $\omega \ll 1$  (section 4.2). In general, both cases display circle map dynamics. In section 4.3 we illustrate the dynamics for intermediate values of  $\omega$  numerically since detailed analytical study appears not to be possible.

#### 4.1 The dynamics for large $\omega$

For the original ODEs (1) we might intuitively expect that, in the limit  $\omega \rightarrow \infty$ , the time-periodic forcing term has an effect equivalent to that of the time-averaged perturbation term  $\gamma(1-x)/2$ .

From (11)<sub>1</sub>, recalling that  $a_1 = c^2/(c^2 + 4\omega^2)$ ,  $b_1 = 2c\omega/(c^2 + 4\omega^2)$ ,  $a_2 = e^2/(e^2 + 4\omega^2)$ , and  $b_2 = 2e\omega/(e^2 + 4\omega^2)$ , we deduce that, as  $\omega \rightarrow \infty$ ,  $\bar{x} \approx \mu_1\gamma + O(\gamma/\omega)$ . Substituting this into (11)<sub>2</sub> indicates that the return time  $T = \bar{t} - t$  becomes

$$\begin{aligned} T &= \mu_3 - \xi \log(\mu_1\gamma + O(\gamma/\omega)) - \gamma\xi/(2e) [\mu_1\gamma + O(\gamma/\omega)]^{-1}, \\ &= \mu_3 - \xi/(2e\mu_1) - \xi \log(\mu_1\gamma) + O(\gamma/\omega), \\ &\sim C_1 - C_2 \log \gamma, \end{aligned}$$

where  $C_1 = \mu_3 - \xi/(2e\mu_1) - \xi \log \mu_1$  and  $C_2 = \xi$  are constants. The result of this calculation is therefore exactly that discussed above in section 2.2 and illustrated in figure 1.

We turn now to the dynamics of (11) for finite  $\omega$ . Substituting  $x = \mu_1\gamma$  into (11)<sub>2</sub> we obtain

$$\begin{aligned} \bar{t} &= t + \mu_3 - \xi \log(\mu_1\gamma) - \frac{\xi}{2e\mu_1} (1 - \sqrt{a_2} \sin(2\omega t)), \\ &= t + \nu + \frac{\xi\sqrt{a_2}}{2e\mu_1} \sin(2\omega t), \end{aligned}$$

where for convenience we define the constant  $\nu = \mu_3 - \xi \log(\mu_1\gamma) - \frac{\xi}{2e\mu_1}$ . We tidy up by rescaling time, letting  $s = \frac{\omega}{\pi}t$ , and observing that  $\sqrt{a_2} \sim \frac{e}{2\omega}$  when  $\omega \gg 1$ . We obtain

$$\begin{aligned} \bar{s} &= s + \frac{\omega}{\pi}\nu + \frac{\xi\omega\sqrt{a_2}}{2\pi e\mu_1} \sin(2\pi s), \\ &\approx s + \frac{\omega}{\pi}\nu + \frac{\xi}{4\pi\mu_1} \sin(2\pi s), \end{aligned} \tag{12}$$

which is the canonical 2-parameter family of circle maps

$$\bar{\theta} = \theta + \alpha + \frac{\beta}{2\pi} \sin(2\pi\theta),$$

which are invertible if  $\beta < 1$  and noninvertible if  $\beta > 1$ . Comparing (12) to the canonical family, we see that passing to the limit  $\omega \rightarrow \infty$  is equivalent to letting  $\alpha \rightarrow \infty$  at fixed  $\beta = \xi/(2\mu_1)$  in the canonical family. Therefore, we have proved the following proposition:

**Proposition 4.1** *For large  $\omega$  there exists a constant  $K$  near  $\xi/2$  such that (i) if  $\mu_1 > K$  then system (3) is equivalent to the canonical family of invertible circle maps, and (ii) if  $\mu_1 < K$  then it is equivalent to a family of noninvertible circle maps.*

The reduction to a circle map indicates that there is an invariant curve for the 2D map; to a first approximation it is just the horizontal line  $x = \mu_1\gamma$  in the  $(t, x)$  plane. Fixed points for the circle map correspond to periodic orbits near the RHC for the ODEs (1). Proposition 4.1 indicates whether the circle map is expected to be invertible or non-invertible; this depends on the ratio  $\xi/(2\mu_1)$ .  $\xi$  depends only on the eigenvalues  $c$  and  $e$ , but  $\mu_1$  depends on the global parts of the dynamics, away from neighbourhoods of the equilibria; these will also vary if we vary  $c$  and  $e$ . So it is not possible to conclude directly, for example, that if  $c$  and  $e$  are large (so that  $\xi$  is small) then  $\beta$  will be less than unity, and the circle map will be invertible.

## 4.2 The dynamics for $\omega$ near 0

In this section we consider the opposite limiting case, i.e.  $\omega \rightarrow 0$ . We recall that  $a_1 = c^2/(c^2 + 4\omega^2)$  and  $a_2 = e^2/(e^2 + 4\omega^2)$  so they both tend to unity as  $\omega \rightarrow 0$ . In addition,  $b_1 = 2c\omega/(c^2 + 4\omega^2)$  and  $b_2 = 2e\omega/(e^2 + 4\omega^2)$  both tend to zero as  $\omega \rightarrow 0$ . The map (11) can then be easily simplified by dropping the terms with coefficients  $b_1$  and  $b_2$ . Comparisons with numerical simulations show that an even simpler nonlinearity is sufficient to capture the dynamics at small  $\omega$ . Iterates of the map lie close to an invariant curve that can be well approximated by  $x = \mu_1\gamma(1 - \sqrt{a_1} \cos(2\omega t))$ . Substituting this expression for  $x(t)$  into (11), the dynamics can be reduced to the circle map

$$\bar{t} = t + \nu - \xi \log(1 - \sqrt{a_1} \cos(2\omega t)),$$

where the constant  $\nu = \mu_3 - \xi \log(\mu_1\gamma) - \frac{\xi}{2e\mu_1}$ . For convenience we rescale  $t$  by writing  $s = \frac{\omega}{\pi}t$  so that the circle map becomes

$$\bar{s} = h(s) := s + \frac{\omega}{\pi}\nu - \frac{\omega}{\pi}\xi \log(1 - \sqrt{a_1} \cos(2\pi s)). \quad (13)$$

Figure 12 shows that the dynamics of (13) match the dynamics of the ODEs very well. We observe the existence of a sequence of intervals in  $\omega$  containing period  $n$  orbits, apparently for all natural numbers  $n$  in order, as  $\omega$  decreases to zero. The maximum return time of orbits appears to increase without bound as  $\omega \rightarrow 0$ , indicating that this is a different regime of circle map dynamics to that investigated at large  $\omega$ . The constants in (13) were set to the values  $\mu_1 = 9.6$  and  $\mu_3 = 17$ . At  $c = 0.25$ ,  $e = 0.2$  and  $\gamma = 10^{-6}$ , therefore we obtain  $\xi = 19.1$  and  $\nu = 232.3$ .

For example, equation (13) possesses the property that there are no values of  $\omega$  for which it is a homeomorphism of the circle. More precisely, we can compute directly that the equation  $h'(s) = 1 - \frac{2\omega\xi\sqrt{a_1}\sin(2\pi s)}{1 - \sqrt{a_1}\cos(2\pi s)} = 0$  has a solution for all  $\omega$ :  $h'(s) = 0$  if and only if

$$\sqrt{a_1} \cos(2\pi s) + 2\omega\xi\sqrt{a_1} \sin(2\pi s) = 1,$$

which holds if  $a_1 + 4\omega^2\xi^2a_1 > 1$ . This inequality simplifies to demanding  $c\xi > 1$ . Since  $c\xi = (c/e)(1 + c/e + (c/e)^2) > 3$  the inequality holds (for all  $\omega$ ) throughout the parameter regime of interest (where  $c/e > 1$  always).

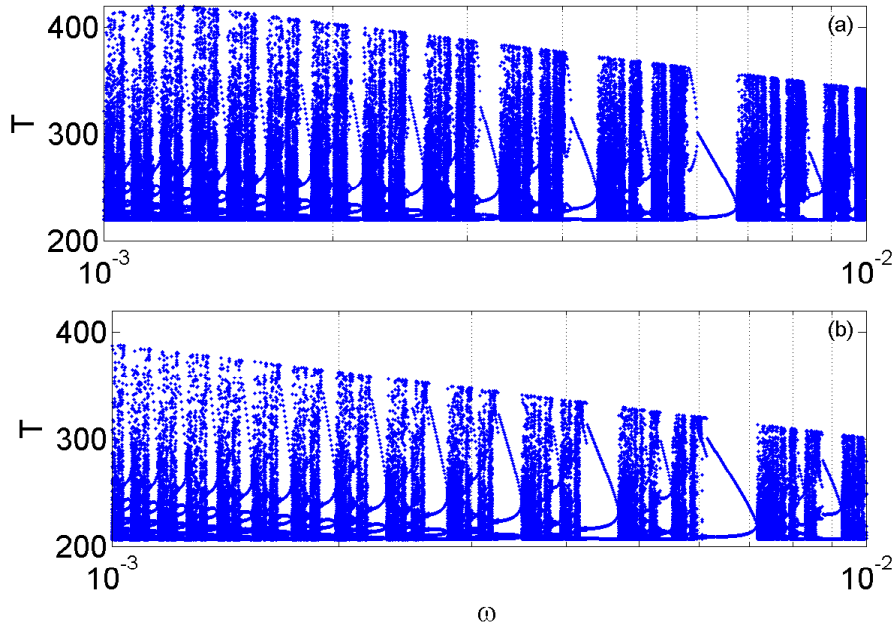


Figure 12: Dynamics for  $\omega \in [10^{-3}, 10^{-2}]$  for (a) the map (13) and (b) the ODEs (1). Periodic solutions of increasing periods appear as  $\omega$  decreases. Each period- $k$  solution appears in a saddle-node bifurcation and then appears to undergo a sequence of period-doubling bifurcations. This is an indication that the systems display quantitatively identical chaotic dynamics over intervals in  $\omega$ . Parameter values are  $c = 0.25$ ,  $e = 0.2$ , and  $\gamma = 10^{-6}$ , and for the map  $\mu_1 = 9.6$ ,  $\mu_3 = 17$ ; and therefore  $\nu = 232.3$ . 50 points are plotted for each of  $10^3$  values of  $\omega$ , logarithmically equally spaced over the interval  $[10^{-3}, 10^{-2}]$ .

Noninvertible circle maps of this kind demonstrate more complicated, and often chaotic, dynamics as compared to their homeomorphism counterparts. A central observation is that, for fixed coefficients, they may not possess a unique rotation number but instead have a continuum of rotation numbers; a *rotation interval*.

We recall the definition of the *rotation number* of an orbit of a  $C^1$  circle map  $f : S^1 \rightarrow S^1$  with initial point  $s_0 \in S^1$ :

$$\rho(f, s_0) = \lim_{n \rightarrow \infty} \frac{f^n(s_0) - s_0}{n}.$$

Rotation numbers form a closed subset of  $[0, 1]$ , and for monotone maps, i.e. those satisfying  $f'(s) \geq 0$ , it can be shown that the rotation number is unique, i.e. independent of the choice of initial condition  $s_0$ . For non-monotone circle maps we may not have uniqueness, and hence an interval of rotation numbers may exist ([29, 27, 8]). Assuming that  $f$  is orientation-preserving, the rotation interval for  $f$  is defined by  $\rho(f) = [\rho(f_-), \rho(f_+)]$ , where  $f_-(s) := \inf_{y \geq s} \{f(y)\}$  defines a monotone function which is pointwise less than or equal to  $f(s)$  and, likewise,  $f_+(s) := \sup_{y \leq s} \{f(y)\}$  defines a monotone function which is pointwise greater than or equal to  $f(s)$ . Since  $f_-$  and  $f_+$  are (from the definitions) monotone,  $\rho(f_-)$  and  $\rho(f_+)$  must themselves be single values, not intervals.

For any rotation number within the rotation interval  $\rho(f)$  there exists an initial point  $s_0$  whose orbit has that rotation number. Since orbits are periodic if and only if they have rational rotation numbers, the existence of a rotation interval implies the existence of countably many periodic orbits at that parameter value.

Figure 13 illustrates the appearance of rotation intervals for the map (13), indicating the intervals in  $\omega$  over which (13) has infinitely many periodic solutions. We compute figure 13 by calculating numerically the rotation numbers of  $f_-$  and  $f_+$  for each  $\omega$ .

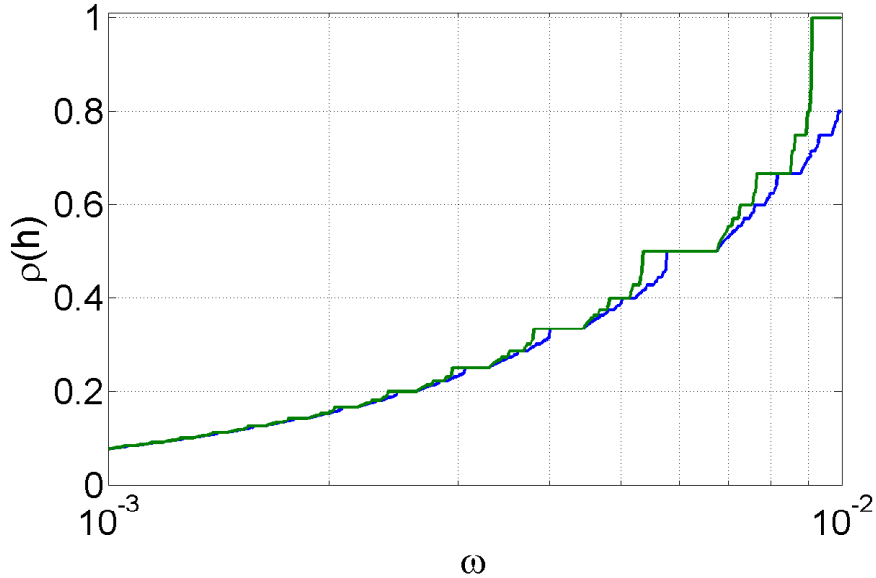


Figure 13: Rotation intervals for the map  $h(s)$ , defined in (13). The figure shows the maximum (green) and minimum (blue) rotation numbers possible at each  $\omega$ . The existence of a nontrivial rotation interval indicates the existence of infinitely many periodic solutions at this value of  $\omega$ .

Moreover, MacKay and Tresser [26] proved that the existence of a non-trivial rotation interval for  $f$  implies topological chaos. Therefore (13) certainly has chaotic dynamics at those values of  $\omega$  for which it has a non-trivial rotation interval. Of course, this condition is sufficient but not necessary: there may also be (unstable) chaotic invariant sets at other values of  $\omega$ , where for example they coexist with an attracting periodic orbit.

Figure 14 illustrates the Arnol'd tongue structure for the 2-parameter map  $\bar{s} = \phi_{\alpha,\beta}(s) \equiv s + \alpha - \beta \log(1 - \sqrt{a_1} \cos(2\pi s))$  where we define  $a_1 = c^2/(c^2 + 4(\pi\beta/\xi)^2)$ . As already discussed, the form of the nonlinearity makes the map  $\phi_{\alpha,\beta}(s)$  noninvertible for all positive values of  $\beta$ . The red curves in figure 14, computed numerically, indicate the locations of saddle-node bifurcations for the first few periodic orbits of interest: a period- $n$  orbit with rotation number  $\rho = 1/n$  exists between the curves labelled  $P_n^+$  and  $P_n^-$  which meet at the point  $(1/n, 0)$  on the  $\alpha$ -axis. The purple curves  $H_n$  indicate the location of homoclinic bifurcations involving the period- $n$  orbit. As discussed in [8], a homoclinic bifurcation occurs when the set of preimages of an unstable period- $n$  orbit of a map contains the critical point (i.e. its minimum or maximum), and this homoclinic bifurcation gives rise to chaotic dynamics. To understand the dynamics of our original map  $h(s)$ , defined in equation (13), we therefore follow the one-parameter family indicated by the sloping blue line on which  $\beta = \xi\alpha/\nu$ . Equivalently, points on this line are parameterised by  $\omega$  since  $\alpha = \omega\nu/\pi$  and  $\beta = \omega\xi/\pi$ . Putting together information from figures 13 and 14 indicates that, as  $\omega \rightarrow 0$ , each period- $n$  solution exists over an interval  $\alpha \in [P_n^-, P_n^+]$  and infinitely many periodic solutions appear and coexist when  $\alpha \in [P_n^-, H_n)$ . This period- $n$  orbit then disappears when we cross the line  $P_n^-$  with  $\alpha$  and  $\beta$  decreasing.

This intuition from numerical computations can be confirmed analytically by considering the dynamics of the 2-parameter map  $\phi_{\alpha,\beta}(s)$  at small  $\beta$ . More precisely, we can show that for all integer  $n$  there exists an interval in  $\omega$  within which a period- $n$  orbit exists, as follows. Consider the 2-parameter circle map  $\phi_{\alpha,\beta}(s) \equiv s + \alpha + \beta p(s)$ , where  $p(s)$  is 1-periodic. It is clear that a period  $n$  solution exists when  $\alpha = 1/n$  and  $\beta = 0$ . We therefore Taylor expand  $\alpha = 1/n + a\beta + b\beta^2 + O(\beta^3)$  and estimate the region of the  $(\alpha, \beta)$

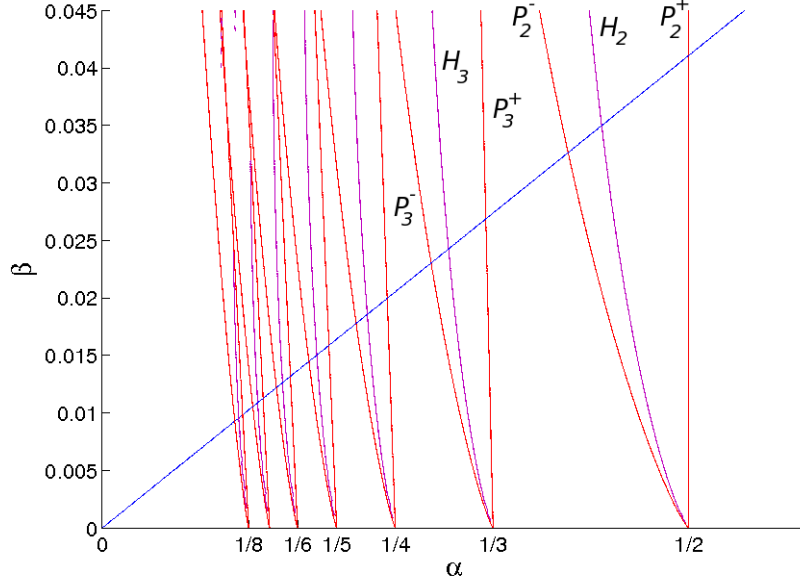


Figure 14: The boundary curves of the Arnol'd tongues ( $P_n^-$  and  $P_n^+$ , red) and the homoclinic bifurcation curves ( $H_n$ , purple) of the map  $\phi_{\alpha,\beta}(s)$ . The diagonal (blue) line  $\beta = \xi\alpha/\nu$  indicates the set of points for which  $(\alpha, \beta) = (\frac{\omega}{\pi}\nu, \frac{\omega}{\pi}\xi)$ , which describes the case of the map (13). Period- $n$  solutions exist along segments of the blue line that lie between  $P_n^-$  and  $P_n^+$ . Infinitely many periodic solutions exist on the segments of the blue line that lie between  $P_n^-$  and  $H_n$ .

within which a period- $n$  orbit exists. By induction we see that

$$\phi^n(s) = s + n\alpha + \beta \left( \sum_{k=0}^{n-1} p(\phi^k(s)) \right).$$

Substituting the above Taylor expansion for  $\alpha$  into the equation  $\phi^n(s) = s + 1$ , we obtain

$$a = -\frac{1}{n} \sum_{k=0}^{n-1} p\left(s + \frac{k}{n}\right) \quad \text{and} \quad b = -\frac{1}{n} \sum_{k=1}^{n-1} p'\left(s + \frac{k}{n}\right) \left( ka + \sum_{l=0}^{k-1} p\left(s + \frac{l}{n}\right) \right).$$

Since in our case  $\alpha = \omega\nu/\pi$ ,  $\beta = \omega\xi/\pi$  and  $p(s) = -\log(1 - \sqrt{a_1} \cos(2\pi s))$  we see that the approximation  $\alpha = 1/n + a\beta + O(\beta^2)$  yields the following necessary condition for the existence of a period- $n$  orbit, up to  $O(\omega^2)$ ; there exists a period- $n$  orbit if there exists  $s$  that satisfies

$$\frac{\omega}{\pi}\nu = \frac{1}{n} + \frac{1}{n} \sum_{k=0}^{n-1} \log\left(1 - \sqrt{a_1} \cos\left(2\pi\left(s + \frac{k}{n}\right)\right)\right) \frac{\omega\xi}{\pi}.$$

Rearranging, we write this condition as

$$\left(\frac{\omega\nu}{\pi} - \frac{1}{n}\right) \frac{n\pi}{\omega\xi} = \sum_{k=0}^{n-1} \log\left(1 - \sqrt{a_1} \cos\left(2\pi\left(s + \frac{k}{n}\right)\right)\right). \quad (14)$$

A necessary condition for the existence of a period- $n$  solution can now be deduced by considering upper and lower bounds for the right-hand side of (14). Expanding  $\sqrt{a_1} = 1 - 2\omega^2/c^2 + O(\omega^4)$  up to the same

order of approximation as used in (14), and substituting, we see that

$$n \log \left( \frac{2\omega^2}{c^2} \right) \leq \sum_{k=0}^{n-1} \log \left( 1 - \sqrt{a_1} \cos \left( 2\pi \left( s + \frac{k}{n} \right) \right) \right) \leq n \log 2. \quad (15)$$

The first of these inequalities leads to the (implicit) lower bound

$$2\xi\omega \log \omega + \frac{\pi}{n} \leq \omega \left[ \nu - \xi \log (2/c^2) \right], \quad (16)$$

while the second inequality leads to the upper bound

$$\omega \leq \frac{\pi}{n(\nu - \xi \log 2)}. \quad (17)$$

These inequalities are consistent with the numerical computations presented in figure 14; in this specific case we have  $\nu \approx 232.3$  which is much larger than  $\xi \log 2 \approx 19.1$  and so (17) describes the near-vertical right-hand sides of the tongues, while (16) describes the clearly more curved left-hand sides.

### 4.3 The dynamics for intermediate values of $\omega$

Within our original Poincaré map (11), there are two sources of nonlinearity: the terms with the coefficient  $\mu_2$  that depend on the combination  $g$  originate in the local maps that we constructed to describe the dynamics in the neighbourhoods of the axes, while the terms with coefficients  $\mu_4$  and  $\mu_5$ , containing  $\omega \bar{t}$  originate in the global maps.

For values of  $\omega$  that are not obviously close either to the limit of small or large  $\omega$ , the dynamics of (11) are affected in complicated ways by the combination of terms originating in the local and global parts of the Poincaré map construction and it is not clear how to further simplify the form of our Poincaré map. Therefore our discussion in this section will rest in large part on numerical results. Figure 15 shows numerical simulations of the underlying time-periodically forced ODE system and the iteration of the 2D Poincaré map (11) in the case :  $c = 0.25$ ,  $e = 0.2$  and  $\gamma = 10^{-6}$ . For the map we choose the parameter values  $\mu_1 = 9.6$ ,  $\mu_2 = 0.3$ ,  $\mu_3 = 17$ ,  $\mu_4 = 26.4$  and  $\mu_5 = -35.7$ ; there is clearly extremely good quantitative agreement, notwithstanding the fact that there are five undetermined parameters. In the intermediate regime, the main features of the dynamics of the ODEs (1) as well as the Poincaré map (11) are a sequence of non-overlapping intervals in  $\omega$  within which we clearly have frequency-locking, and separated by regions within which there are complicated, possibly chaotic, dynamics. At the ends of the frequency-locking intervals, the periodic orbit undergoes a saddle-node bifurcation and then disappears. There is no bistability, and the dynamics is that of a circle map. Figure 16 confirms this assertion: denoting  $t_n \bmod \pi/\omega$  by  $t_n$  for simplicity, we plot  $t_{n+1}$  against  $t_n$  for fixed  $\omega = 0.0428$ ,  $c = 0.25$  and  $e = 0.2$  (other parameter values are the same as in Figure 15).

In section 4.1 and 4.2 we have shown that our Poincaré map is well approximated by different families of circle maps in different limits:  $\bar{s} = s + \frac{\omega}{\pi}\nu + \frac{\xi}{4\pi\mu_1} \sin(2\pi s)$  for large  $\omega$ , and  $\bar{s} = s + \frac{\omega}{\pi}\nu - \frac{\omega\xi}{\pi} \log(1 - \sqrt{a_1} \cos(2\pi s))$  for  $\omega$  near 0. There is a transition between these two families when  $\omega$  increases from near 0 to large values. Since our numerical simulations indicate a value for  $\mu_1$  around 9.6, and therefore  $\xi/(2\mu_1) \approx 0.16$ , there is a transition at intermediate  $\omega$  at which the circle map becomes invertible. We remark that the period-doubling bifurcations which can be seen within the frequency-locking intervals at small  $\omega$  in Figure 15 must disappear before the circle map becomes invertible, as  $\omega$  increases; this is a well-known feature of circle map dynamics, see for example [39].

To further examine, numerically, this transition from noninvertible to invertible circle map dynamics we applied the ‘0-1 test for chaos’ developed by G.A. Gottwald and I. Melbourne [15, 16] which distinguishes in a computationally cheap and reliable way between regular and chaotic dynamics in a (low-dimensional) deterministic system. We refer readers to these references for a detailed discussion of the test and the underlying theory. The test indicates a transition at around  $\omega \approx 0.13$  from a noninvertible

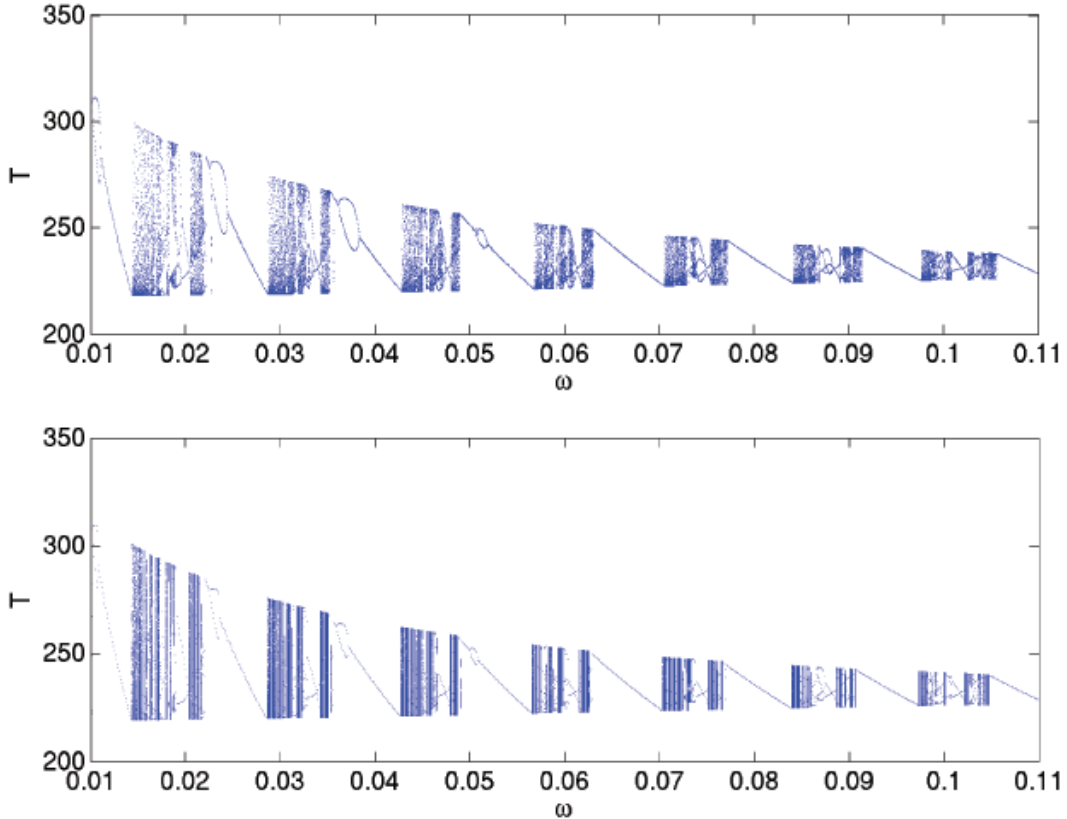


Figure 15: Frequency locking windows for the ODEs (1) (upper plot) and in the Poincaré map (11) (lower plot) when  $c = 0.25$ ,  $e = 0.2$  and  $\gamma = 10^{-6}$ . The parameters in the Poincaré map are:  $\mu_1 = 9.6$ ,  $\mu_2 = 0.3$ ,  $\mu_3 = 17$ ,  $\mu_4 = 26.4$  and  $\mu_5 = -35.7$ .

map at smaller  $\omega$  (i.e. for which the intervals of complicated dynamics between frequency-lockings contain chaotic dynamics) to an invertible one at larger  $\omega$ , for which these intervals between frequency-lockings do not contain chaotic dynamics.

## 5 Discussion

### 5.1 Comparison with the results of Afraimovich et al [2]

In this section we discuss the complementary results obtained by V. S. Afraimovich et al.[2] for a very similar problem. We show that the theorems proved in [2] support our numerical and asymptotic conclusions, and that our results extend the analyses provided there. Specifically, Afraimovich et al considered the dynamics of the ODEs

$$\begin{aligned}
 \dot{x}_1 &= x_1(1 - x_1 - \alpha_1 x_2 - \beta_1 x_3) + \gamma \varphi_1(t) \\
 \dot{x}_2 &= x_2(1 - \beta_2 x_1 - x_2 - \alpha_2 x_3) + \gamma \varphi_2(t) , \\
 \dot{x}_3 &= x_3(1 - \alpha_3 x_1 - \beta_3 x_2 - x_3) + \gamma \varphi_3(t)
 \end{aligned} \tag{18}$$

where the  $\varphi_j(t)$  are smooth and positive  $2\pi$ -periodic functions, so that the octant of  $\mathbb{R}^3$  in which  $x_1, x_2, x_3 > 0$  is forward-invariant for the dynamics. They define the eigenvalues  $\lambda_{j1} = 1 - \beta_j$ ,  $\lambda_{j2} = -1$

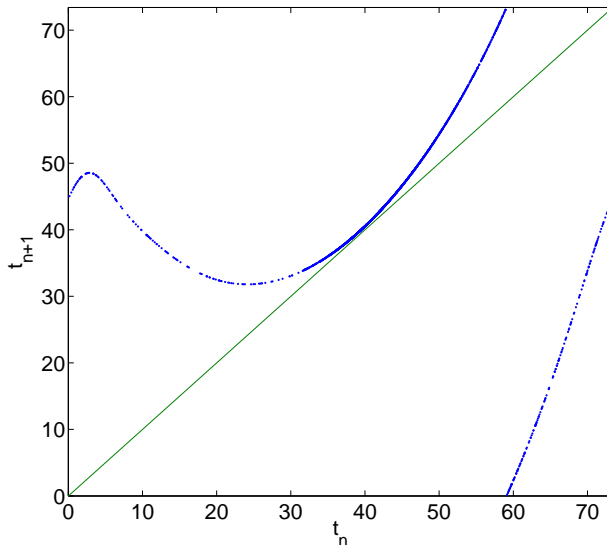


Figure 16: Circle-map-like dynamics in the ODEs (1). We plot  $t_{n+1}$  against  $t_n$  for fixed parameters  $\omega = 0.0428$ ,  $c = 0.25$  and  $e = 0.2$ .

and  $\lambda_{j3} = 1 - \alpha_j$  for  $j = 1, \dots, 3$ . Then the system becomes

$$\begin{aligned} \dot{x}_1 &= x_1(1 - (x_1 + x_2 + x_3) + \lambda_{13}x_2 + \lambda_{11}x_3) + \gamma\varphi_1(t) \\ \dot{x}_2 &= x_2(1 - (x_1 + x_2 + x_3) + \lambda_{21}x_1 + \lambda_{23}x_3) + \gamma\varphi_2(t) , \\ \dot{x}_3 &= x_3(1 - (x_1 + x_2 + x_3) + \lambda_{33}x_1 + \lambda_{31}x_2) + \gamma\varphi_3(t) \end{aligned} \quad (19)$$

which is clearly a generalisation of our problem in which the eigenvalues at each equilibrium point on an axis, when  $\gamma = 0$ , are related to each other by symmetry. Our symmetric version is recovered if we set, for example,  $\lambda_{13} = \lambda_{23} = \lambda_{33} = e > 0$  and  $\lambda_{11} = \lambda_{21} = \lambda_{31} = -c < 0$ . Note that [2] only consider  $2\pi$ -periodic perturbations and do not use the perturbing frequency as a bifurcation parameter as we do; an additional (minor) difference is that we explicitly consider only a perturbation to one variable instead of all three. After some detailed calculations, and implicitly taking the perturbation functions  $\varphi_j(t) \propto \sin t$ , [2] produce the following model 2D map

$$\begin{cases} \bar{x} = A(Bx + \gamma(1 + a \sin t))^d \\ \bar{t} = t + \bar{\omega} - \xi \log(Bx + \gamma(1 + a \sin t)), (\text{mod } 2\pi) \end{cases} , \quad (20)$$

where as before,  $\xi = \frac{e^2 + ce + c^2}{e^3}$  and  $d = (c/e)^3$ .  $A$ ,  $B$  and  $\bar{\omega}$  are positive parameters that depend on local and global characteristics of trajectories in the original ODEs (18) or, equivalently, (19). The parameter  $0 < a < 1$  is the amplitude of the sinusoidal perturbation as it affects the global part of the map from a neighbourhood of the point  $(0, 0, 1)$  to a neighbourhood of  $(0, 1, 0)$ . Interestingly, although perturbations to the other two global maps are included, these perturbations do not contribute at leading order in the return map since the perturbations are contracted as trajectories pass through neighbourhoods of  $(1, 0, 0)$  and  $(0, 0, 1)$ .

In the derivation of (20),  $x$  is a coordinate measuring distance from the unstable manifold of one of the equilibrium points that exist when  $\gamma = 0$ , whereas in our maps  $x$  represents distance to the stable manifold. This difference is purely a matter of definition, and the change of variable  $x = y^d$  applied to (20) transforms it into a map that is close to the form (4). A further point of interest in the derivation is the apparent neglect, in the derivation provided in [2], of the effect of periodic perturbations on the

local maps as well as in the global maps. It is surprising that this omission does not change the form of the return map; in this sense it appears rather robust. However, our calculation is perhaps of broader applicability since Afraimovich’s results are presented always in what we term the strongly attracting, or ‘ $\epsilon$  large’, regime, i.e.  $\gamma^\epsilon \ll 1$  as well as  $\gamma \ll 1$ . In this regime we have discussed reductions of the dynamics to that of a circle map that is non-invertible at small  $\omega$  and invertible at larger  $\omega$ . These observations agree with the first of two theorems that Afraimovich et al prove concerning the dynamics of (20). Using the ‘Annulus Principle’, they prove the following theorem:

**Theorem 5.1** (Afraimovich et al. [2]) *If  $d > 1$ ,  $\gamma \ll 1$  and  $0 < a < 1/(\sqrt{1 + \xi^2})$ , then there is an invariant closed curve as the maximal attractor  $x(t)$  for equation (20).*

We note that the small- $a$  regime corresponds to the case in which the forcing frequency  $\omega$  is large, so this result agrees with our observation that at large  $\omega$  the dynamics is that of an (invertible) circle map.

The second theorem proved by Afraimovich et al. concerns a different regime for the dynamics:

**Theorem 5.2** (Afraimovich et al. [2]) *If  $d > 1$ ,  $\gamma \ll 1$  and  $(\exp(10\pi/\xi) - 1)/(\exp(10\pi/\xi) - (1/10)) < a < 1$ , then there exists robust chaos in the sense of a hyperbolic invariant closed set  $\Lambda$  such that the dynamics on  $\Lambda$  is topologically conjugate to the Bernoulli shift on two symbols.*

That is, for  $a$  sufficiently close to 1 we have chaotic dynamics. Although we do not discuss this regime in detail in this paper, this result confirms our numerical observations, reported in [13] and [41] of two-dimensional chaotic dynamics when the eigenvalue ratio  $c/e$ , equivalently the exponent  $d$ , is sufficiently large, for example the regime denoted ‘Region I’ in [41]. The reliance on the ‘strongly attracting’ limit in [2] means that they did not explore the limit  $\epsilon \ll 1$ ,  $\gamma^\epsilon \sim 1$  in which the bistability that we report in section 3 arises.

## 5.2 Comparison with a heteroclinic system perturbed by constant and periodic forcing

We briefly comment in this section on a straightforward extension of our analysis to the case in which the robust heteroclinic cycle is perturbed by a symmetry-breaking constant term plus a time-periodic perturbation. The case of a constant term alone is well known, and therefore this combination enables us to show how the bifurcation structure we observe in earlier sections is related to the constant perturbation case.

We consider a time-periodic perturbation to the first coordinate in the (more general) form  $(1 - x)(\delta(f(2\omega t) - A) + \gamma A)$  where  $\delta$  and  $\gamma$  are introduced as independent parameters, and  $A = \frac{1}{P} \int_0^P f(t') dt'$  is the time average of  $f$ , assumed periodic with period  $P$ . The system (1) becomes

$$\begin{cases} \dot{x} &= x(1 - (x + y + z) - cy + ez) + (1 - x)(\delta(f(2\omega t) - A) + \gamma A) \\ \dot{y} &= y(1 - (x + y + z) - cz + ex) \\ \dot{z} &= z(1 - (x + y + z) - cx + ey) \end{cases} . \quad (21)$$

In this formulation, for a given  $f$ ,  $\gamma$  describes the amplitude of the constant term in the perturbation, while  $\delta$  controls the amplitude of the time-periodic fluctuations around the constant. When  $\delta = 0$  we have a purely constant perturbation and hence we expect a long-period periodic orbit to form (with a period independent of  $\omega$ ). In the opposite limiting case, where  $\delta = \gamma$ , we recover the original system (1). To preserve the forward-invariance of the positive orthant we restrict our attention to the range  $0 \leq \delta \leq \gamma$ .

In this subsection we briefly show how our results from earlier sections are modified when this new perturbation ansatz is used. The details of the analysis are omitted since in all cases they follow that presented previously.

### 5.2.1 Periodic orbit in the constant perturbation case $\delta = 0$

First we prove that there exists a periodic attractor for  $\delta = 0$ . To derive the Poincaré map in this case we need only to refer to the general expression for the Poincaré map given by (47) in the Appendix, and substitute  $A$  for the function  $f(2\omega t)$ . After straightforward calculation of  $L_1(x, t)$ ,  $L_2(x, t)$  and observing that (since the unstable manifold of  $P'_2$  is time-independent in this case),  $G_1(x, t)$  and  $G_2(x, t)$  are constant, we obtain the Poincaré map

$$\begin{aligned} f_1(x, t) &= \mu x^d + [\nu_3 + \nu_4 x^d] \gamma + O(\gamma^2) \\ &= \mu x^d + \nu_3 \gamma + O(\gamma^{1+d}, \gamma^2), \\ f_2(x, t) &= t + \mu_3 - \xi \log x + \frac{\xi A}{e} (1/h - x) \gamma \\ &= t + \mu_3 - \xi \log x + O(\gamma), \end{aligned} \tag{22}$$

where  $\nu_3$  and  $\nu_4$  are constants. Note that the first component has decoupled at leading order. Therefore, since  $d > 1$  there is clearly an attracting fixed point  $x_0 = f_1(x_0)$  for  $\gamma$  small enough. This implies the existence of a periodic attractor for the corresponding system (21) with period approximately  $\mu_3 - \xi \log x_0$ . For  $\delta > 0$  we therefore expect to have a periodic oscillator that is periodically perturbed.

For comparison with previous sections, we consider the case  $f(2\omega t) = \sin^2(\omega t)$ . Following the method described in detail in the Appendix, the Poincaré map for system (21) with  $f(2\omega t) = \sin^2(\omega t)$  is:

$$\begin{aligned} \bar{x} = f_1(x, t) &= \mu x^d + \gamma \mu_1 + \delta [\mu_2 (-a_1 \cos(2\omega g) - b_1 \sin(2\omega g)) \\ &\quad - \mu_4 (-a_1 \cos(2\omega(\bar{t} - \delta_3)) - b_1 \sin(2\omega(\bar{t} - \delta_3))) \\ &\quad - \mu_5 (-a_2 \cos(2\omega \bar{t}) - b_2 \sin(2\omega \bar{t}))] + O(\gamma^2) \end{aligned} \tag{23}$$

$$\bar{t} = f_2(x, t) = t + \mu_3 - \xi \log(x) - \frac{\xi}{2e} [\gamma - \delta (a_2 \cos(2\omega t) + b_2 \sin(2\omega t))] x^{-1} + O(\gamma^2) \tag{24}$$

We now comment in turn on the strongly and weakly attracting cases in which  $\gamma^\epsilon \ll 1$  ( $\epsilon$  is ‘large’) or  $\gamma^\epsilon \sim 1$  ( $\epsilon$  is near zero), respectively.

### 5.2.2 The strongly attracting case

In the limit in which  $\epsilon$  is of order unity, i.e.  $\gamma^\epsilon \ll 1$ , and when  $\omega$  is small, (23) can be simplified as in section 4.2, noting that the  $x^d$  term can be ignored at leading order, and simplifying the various coefficients, to write  $f_1(x, t)$  in the form

$$\bar{x} = f_1(x, t) = \mu_1 (\gamma - \delta \sqrt{a_1} \cos(2\omega \bar{t})).$$

Substituting this expression for the invariant curve  $x = \mu_1 (\gamma - \delta \sqrt{a_1} \cos(2\omega \bar{t}))$  into (24) and letting  $s = \omega t / \pi$ , we obtain the one dimensional map:

$$\bar{s} = h(s) = s + \frac{\omega}{\pi} \nu - \frac{\omega}{\pi} \xi \log(1 - \gamma^{-1} \delta \sqrt{a_1} \cos(2\pi s)), \tag{25}$$

where  $\nu = \mu_3 - \xi \log(\mu_1 \gamma) - \xi / (2e \mu_1)$ . The map (25) is invertible if and only if the equation  $h'(s) = 0$  has no solution. By direct computation,

$$h'(s) = 1 + \frac{2\omega \xi \gamma^{-1} \delta \sqrt{a_1} \sin(2\pi s)}{1 - \gamma^{-1} \delta \sqrt{a_1} \cos(2\pi s)},$$

and so the condition  $h'(s) = 0$  can be satisfied if and only if

$$(\gamma^{-1} \delta)^2 < \frac{c^2 + 4\omega^2}{c^2 + 4\omega^2 c^2 \xi^2}. \tag{26}$$

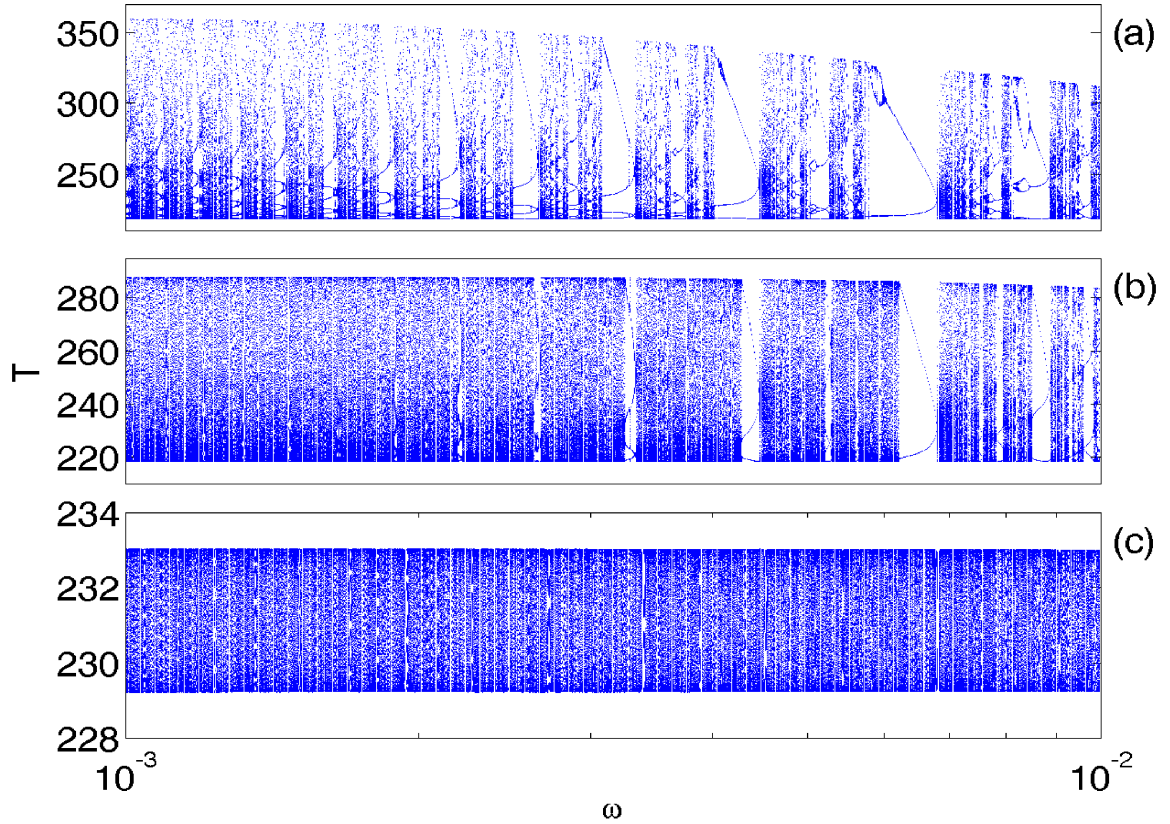


Figure 17: Log-linear plot showing the emergence of frequency locked periodic orbits in (21) at small  $\omega$  as  $\delta$  increases, for  $\gamma = 10^{-6}$ . (a)  $\delta = 9.99 \times 10^{-7} = 0.999\gamma$ ; (b)  $\delta = 9.5 \times 10^{-7} = 0.95\gamma$ , and (c)  $\delta = 10^{-7} = 0.1\gamma$ .

Since the expression on the right-hand-side of (26) tends to unity from below as  $\omega \rightarrow 0$ , we conclude that, given any fixed  $\delta/\gamma < 1$ , (25) is invertible for all sufficiently small  $\omega$ . Moreover, if  $\delta \ll \gamma$ , (25) is very close to the rigid rotation  $\bar{s} = s + \frac{\omega}{\pi}\nu$  and we expect that any periodic solution will exist over an interval in  $\omega$  that has a width that scales linearly with  $\delta$  as  $\delta$  tends to zero. Figure 17(c) illustrates the emergence of frequency-locking and complicated dynamics in (21) as  $\delta$  increases.

We discuss the case  $\omega \rightarrow \infty$  by a similar argument, following section 4.1. Taking  $\omega$  large enough such that  $a_1$  and  $a_2$  are both small, of order  $\gamma$ , we can guarantee that (23) yields  $x \approx \mu_1\gamma$  since both the  $x^d$  term and the  $t$ -dependent terms are smaller. Substituting this into (24), we have

$$\bar{t} = t + \nu + \gamma^{-1}\delta \frac{\xi\sqrt{a_2}}{2e\mu_1} \sin(2\omega t),$$

where  $\nu = \mu_3 - \xi \log(\mu_1\gamma) - \frac{\xi}{2e\mu_1}$ . Since  $\sqrt{a_2} \approx \frac{e}{2\omega}$  when  $\omega$  is large, by letting  $s = \frac{\omega}{\pi}t$ , this equation becomes

$$\bar{s} \approx s + \frac{\omega}{\pi}\nu + \frac{\xi}{4\pi\mu_1}\gamma^{-1}\delta \sin(2\pi s),$$

which is clearly an invertible circle map for all small enough  $\delta$ .

To summarise, we can guarantee that the dynamics of (21), for any fixed  $\delta < \gamma$ , is equivalent to an invertible circle map both for  $\omega$  sufficient close to zero and for  $\omega$  sufficiently large. For intermediate values of  $\omega$  we expect that the map is always invertible for sufficiently small  $\delta$ , but we have not proved this.

### 5.2.3 The weakly attracting case

In the weakly attracting case, in which  $\epsilon$  is small, so that  $\gamma^\epsilon \sim 1$ , we follow the discussion set out in section 3.2 to obtain the following simplification of (23) - (24):

$$\begin{cases} \bar{x} &= \mu x^d + \mu_1 [\gamma + \delta(-a_2 \cos(2\omega t) + b_2 \sin(2\omega t))] \\ \bar{t} &= t + \mu_3 - \xi \log \bar{x} \end{cases},$$

which can be simplified as before, by redefining  $\gamma$  and shifting  $t$  (and absorbing this shift into  $\mu_3$ ), to give

$$\begin{cases} \bar{x} &= \mu x^d + \gamma (1 + \gamma^{-1} \delta \sqrt{a_2} \sin(2\omega t)) \\ \bar{t} &= t + \mu_3 - \xi \log \bar{x} \end{cases},$$

The analysis in section 3.2 for the dynamics within the frequency-locking intervals applies directly here, replacing  $\sqrt{a_2}$  by  $\gamma^{-1} \delta \sqrt{a_2}$ . As a result, (21) is seen to be equivalent to the forced damped pendulum with torque:

$$\ddot{s} + \eta^{-1} \dot{s} + \sqrt{a_2} \sin s = \gamma \delta^{-1} \lambda, \quad (27)$$

where  $\eta^2 = \frac{6\omega \hat{x}}{\gamma e}$  as previously. Referring to Figure 10, if  $|\lambda| < \gamma^{-1} \delta \sqrt{a_2}$  then there is the possibility of frequency locking. If  $|\lambda| > \gamma^{-1} \delta \sqrt{a_2}$  then the only attractor for (27) is a stable periodic orbit. In the same way as noted above, the width of these intervals of frequency locking also decreases linearly with  $\delta$ .

## 6 Conclusion

In this paper we discuss the dynamics in the vicinity of a robust heteroclinic cycle perturbed by a small amplitude time-periodic forcing function. Given the well known analyses of perturbations of robust heteroclinic cycles by both constant terms and in the presence of noise, it is perhaps surprising that so few papers consider the periodically forced case. We present analytic and numerical studies of the dynamics of our model system which is based on the traditional Guckenheimer–Holmes heteroclinic cycle, perturbed externally by a non-negative time-periodic forcing function with amplitude  $\gamma$ . The rationale for these specific choices are that they are the simplest situation, avoiding switching around heteroclinic networks, or at least around group orbits of heteroclinic cycles, and the availability of previous work by other authors for comparison. We use the frequency  $\omega$  of the perturbation function as the principle bifurcation parameter; the second key parameter is the saddle index  $d$  of the robust heteroclinic cycle. Our results provide explanations of the frequency-locking phenomena reported by earlier authors, in particular by Rabinovich *et al* [35].

We begin by presenting a systematic calculation of the Poincaré map for the robust heteroclinic cycle subjected to a non-negative periodic forcing function  $f(2\omega t)$ . By including the time-dependent terms through all steps in the calculation, we obtain Poincaré map that can be quantitatively compared to the dynamics of the original non-autonomous differential equations. The comparison shows that the return map captures the dynamics strikingly well.

Our results, together with those of Afraimovich *et al* [2] and our earlier work [13] show that there are three distinct regimes for the dynamics, in terms of the two parameters  $\gamma$  and  $\epsilon := d - 1 > 0$ .  $\epsilon$  measures the strength of attraction of the robust heteroclinic cycle in the absence of perturbations. Without perturbations, the case  $\epsilon = 0$  corresponds to a resonant bifurcation of the robust heteroclinic cycle. The key results of the paper concern two of the three regimes: throughout the paper we consider the perturbation amplitude  $\gamma$  to be sufficiently small that  $O(\gamma^2)$  contributions are negligible. But there remains the question of distinguished limits and interplay between the two small parameters  $\gamma$  and  $\epsilon$ . We define a ‘weakly attracting’ case through a distinguished limit in which  $\epsilon$  becomes small at a sufficiently fast rate that  $\gamma^\epsilon \sim 1$  in the limit  $\gamma \rightarrow 0$ . Informally we refer to this as considering ‘ $\epsilon$  near 0’. We define a ‘strongly attracting’ case through the limit in which  $\epsilon$  is held fixed as  $\gamma \rightarrow 0$ . This is informally referred to as the case ‘ $\epsilon$  of order unity’. More technically, the ‘ $\epsilon$  near 0’ regime arises when, for a given  $\gamma$ ,  $\epsilon$  is

small enough that the  $x^d$  term in the first coordinate of the Poincaré map plays a leading-order role. In other words the two cases are distinguished asymptotically by the size of  $\gamma^\epsilon$ : either both quantities are close to zero, such that  $\gamma^\epsilon \sim 1$  or  $\epsilon$  is large enough that  $\gamma^\epsilon \ll 1$ .

In the weakly attracting case the map contains both stable fixed points and stable 1-dimensional invariant curves; the dynamics essentially alternates between these as  $\omega$  varies. Thus for the non-autonomous ODEs, orbits may either fluctuate by small amounts near the periodic orbit of an amplitude that would be anticipated from considering just the time-averaged value of the forcing function, or orbits may be frequency-locked and have a period that varies substantially away (both above and below) the period that one would expect from the time-averaged forcing function. This behaviour in some sense demonstrates the sensitivity of the robust heteroclinic cycle, near the resonant bifurcation, to perturbations; periodic orbits with wide variation in periods may exist even if the system parameters are varied only by small amounts. It is also possible that these two scenarios (frequency-locked periodic orbits and orbits that fluctuate close to the period expected from the time-averaged estimate) overlap as  $\omega$  is varied; substantial bistability arises. We explain how this can come about by showing that the model map, and therefore the original ODE problem, can be reduced to a second-order nonlinear ODE describing a damped pendulum with constant torque; this is a well known nonlinear oscillator problem.

In the strongly attracting case, for which  $\epsilon$  remains fixed in the limit  $\gamma \rightarrow 0$  so that  $\gamma^\epsilon \ll 1$ , the bistability described for the weakly attracting case disappears. We observe dynamics that is typical of a circle map, see, for example, Figure 15. We show the equivalence of the dynamics to that of a circle map, and we discuss whether the circle map is likely to be invertible or non-invertible; this depends on  $\omega$  and the parameters in the map. For large enough  $\omega$  we show that the circle map will be invertible and so the complicated dynamics indicated there may be quasiperiodic but is not chaotic. At small  $\omega$  we present strong numerical evidence for the existence of chaos through estimation of the form of the map, showing directly that it is non invertible, through applying the ‘0-1 test’ for chaos and through the direct calculation of non-trivial rotation intervals that are another sufficient condition for the existence of chaotic dynamics.

We compare our results with those found in previous work in section 5.1; these results are largely complementary. Afraimovich et al. [2] showed the existence of the regime we refer to as the strongly attracting case and showed the existence of a third regime, in which chaotic dynamics arises for the two-dimensional return map. This third regime was noted in our previous work [13] and we do not discuss it in detail here. Afraimovich et al. did not discuss the weakly attracting case; the existence and analysis of this regime is novel. We also provide a more detailed study of the strongly attracting regime, using the forcing frequency  $\omega$  as our principal bifurcation parameter. More generally, the comparison with the results of Afraimovich et al [2] links our work to the Poincaré maps used to describe the dynamics near a periodically-perturbed homoclinic orbit in a non-symmetric continuous time dynamical system. A review of this theory is given by Shilnikov et al. [39]; for such a case, they argue that the dynamics are generically described by 2D maps of the form (20). After applying the Annulus Principle they present the different routes by which the dynamics may become chaotic, and described by non-invertible circle maps. We conclude that the dynamics near RHCs has qualitative features in common with that near homoclinic orbits in general, at least in the strongly attracting regime. Bifurcation diagrams very similar to those we compute in figure 15 have been observed experimentally, for example in digital phase-locked loops, as discussed by Lichtenberg and Lieberman [25] (see their section 7.4, pp 532–536 and references therein).

In section 5.2 we link our results with those of a robust heteroclinic cycle perturbed only by a constant, time-independent perturbation. We show that when the amplitude of the time-dependent fluctuations is reduced below the amplitude of the constant part of the perturbation, the widths of the frequency-locking intervals, and the variation in possible periods of orbits to which frequency-locking may occur, shrinks rapidly. We conclude that it is the feature of this forcing term, having fluctuations that are as large as its mean, that allows the wide range of dynamical behaviour that we observe and analyse here.

Many questions remain for future work; some are highlighted above. One obvious question is to remove the non-negativity constraint on the forcing function and allowing trajectories to switch around a

heteroclinic network. Questions concerning the quantitative effect of different forcing terms would also be of interest; in the limit one might imagine a periodic sequence of sharp pulses that would allow an accurate estimation of a, perhaps simpler, Poincaré map in the limit of Dirac delta functions. More broadly, given that one might initially anticipate circle-map-like dynamics for the periodic perturbation of a RHC, the weakly attracting regime might well arise in more complex problems, with circle map dynamics near heteroclinic cycles only when they are well away from resonant bifurcations. More surprising still is the presence of chaotic dynamics in the 2D return map when the RHC is even more strongly attracting. It would be of substantial interest to see if these three regimes (which individually are quite generic kinds of dynamical system) arise in other perturbed RHC problems.

## Acknowledgements

The authors would like to thank Michael Proctor and Alastair Rucklidge for helpful discussions, and two anonymous referees for many useful and constructive comments that helped greatly to improve the presentation of this work. TLT acknowledges funding from the NSC. JHPD currently holds a University Research Fellowship from the Royal Society.

## Appendix

In this appendix we present a detailed derivation of the Poincaré map for the system (1):

$$\begin{cases} \dot{x} &= x(1 - (x + y + z) - cy + ez) + \gamma(1 - x)f(2\omega t) \\ \dot{y} &= y(1 - (x + y + z) - cz + ex) \\ \dot{z} &= z(1 - (x + y + z) - cx + ey) \end{cases},$$

where  $f$  is a continuously differentiable non-negative  $2\pi$ -periodic function,  $0 < \gamma \ll 1$  and  $0 < e < c < 1$ .

Let the two cross sections near  $P_1 = (1, 0, 0)$  be

$$H_1^{in} = \{(x, y, z) : |x - 1| \leq h, 0 \leq y \leq h, z = h\},$$

and

$$H_1^{out} = \{(x, y, z) : |x - 1| \leq h, y = h, 0 \leq z \leq h\},$$

where  $h$  is a small constant. We define cross sections near  $P_2 = (0, 1, 0)$  and  $P_3 = (0, 0, 1)$  similarly, see Figure 2. We construct local maps by integrating the linearisations of the dynamics near  $P_1, P_2$  and  $P_3$ , and we estimate global maps by using  $C^1$ -diffeomorphisms between neighbourhoods of the  $P_j$ . At each step, we calculate not only the point where an orbit hits each cross section but also the length of time that the orbit takes between cross sections. Although the time spent on global parts of the Poincaré map is small compared with the time spent near the points  $P_j$ , especially when  $\gamma$  is small, it is taken into account in the calculations: we denote the time (to leading order in  $\gamma$ ) that elapses during the global maps by the three constants  $\delta_1, \delta_2$  and  $\delta_3$ .

For each local and global map we compute the terms at leading order and at  $O(\gamma)$ . For notational convenience, variables without suffices will be treated as depending only on time  $t$ . Variables with suffices, corresponding to values of the variables on a cross section, will be treated as functions of  $\gamma$ .

### A.1 The local map $H_3^{in} \rightarrow H_3^{out}$

We begin by deriving the local map from  $H_3^{in}$  to  $H_3^{out}$ . Let  $(x_1, h, z_1) \in H_3^{in}$ , near  $P_3$ , be the initial point of a specific orbit at the initial time  $t = s$ . Suppose that this orbit intersects  $H_3^{out}$  at  $(h, y_2, z_2)$  at time

$t = T_1(\gamma)$ . Since the trajectory is close to  $P_3$ , we write  $z(t) = 1 + w(t)$  and set  $z_1 = 1 + w_1$ . The linearized system is

$$\begin{cases} \dot{x} &= ex + \gamma f(2\omega t) \\ \dot{y} &= -cy \\ \dot{z} &= \dot{w} = -w - (1+c)x + (e-1)y \end{cases}$$

Integrating this system from  $H_3^{in}$  to  $H_3^{out}$ , we obtain

$$\begin{cases} h &= x_1 e^{e(T_1(\gamma)-s)} \left( 1 + \gamma \frac{1}{x_1} \int_s^{T_1} e^{-e(\tau-s)} f(2\omega\tau) d\tau \right) \\ y_2 &= h e^{-c(T_1(\gamma)-s)} \\ w_2 &= w_1 e^{-(T_1(\gamma)-s)} \left( 1 + \frac{1}{w_1} \int_s^{T_1} e^{\tau-s} (-(1+c)x(\tau) + (e-1)y(\tau)) d\tau \right) \end{cases} \quad (28)$$

From the first equation of (28) it is clear that (setting  $\gamma = 0$ )

$$T_1(0) = s + \log(h/x_1)^{1/e}. \quad (29)$$

Differentiating the first equation of (28) with respect to  $\gamma$  and setting  $\gamma = 0$ , we get

$$0 = ee^{e(T_1(0)-s)} x_1 T_1'(0) + e^{e(T_1(0)-s)} \int_s^{T_1(0)} e^{-e(-s+\tau)} f(2\omega\tau) d\tau,$$

which implies

$$T_1'(0) = -x_1^{-1} \frac{1}{e} \int_s^{T_1(0)} e^{-e(\tau-s)} f(2\omega\tau) d\tau. \quad (30)$$

Hence we obtain

$$T_1(\gamma) = s + \log\left(\frac{h}{x_1}\right)^{1/e} - \gamma \left[ x_1^{-1} \frac{1}{e} \int_s^{T_1(0)} e^{-e(\tau-s)} f(2\omega\tau) d\tau \right] + O(\gamma^2).$$

Similarly, from the second equation of (28), we can easily verify that  $y_2|_{\gamma=0} = h(h/x_1)^{-c/e}$  and

$$y_2'(0) = h e^{-c(T_1(0)-s)} (-c T_1'(0)) = x_1^{-1+c/e} \left(\frac{c}{e}\right) h^{1-c/e} \int_s^{T_1(0)} e^{-e(\tau-s)} f(2\omega\tau) d\tau. \quad (31)$$

Therefore

$$y_2(\gamma) = h^{1-c/e} x_1^{c/e} + \gamma \left[ x_1^{-1+c/e} \left(\frac{c}{e}\right) h^{1-c/e} \int_s^{T_1(0)} e^{-e(\tau-s)} f(2\omega\tau) d\tau \right] + O(\gamma^2).$$

To derive  $w_2(\gamma)$ , we first note that, (using integration by parts)

$$\begin{aligned} \int_s^{T_1(\gamma)} e^{\tau-s} x(\tau) d\tau &= e^{\tau-s} x(\tau) \Big|_s^{T_1(\gamma)} - \int_s^{T_1(\gamma)} e^{\tau-s} \dot{x}(\tau) d\tau \\ &= e^{T_1(\gamma)-s} h - x_1 - \int_s^{T_1(\gamma)} e^{\tau-s} x(\tau) d\tau - \gamma \int_s^{T_1(\gamma)} e^{\tau-s} f(2\omega\tau) d\tau, \end{aligned}$$

and

$$\begin{aligned} \int_s^{T_1(\gamma)} e^{\tau-s} y(\tau) d\tau &= e^{\tau-s} y(\tau) \Big|_s^{T_1(\gamma)} - \int_s^{T_1(\gamma)} e^{\tau-s} \dot{y}(\tau) d\tau \\ &= e^{T_1(\gamma)-s} y_2(\gamma) - h + c \int_s^{T_1(\gamma)} e^{\tau-s} y(\tau) d\tau. \end{aligned}$$

Tidying up, we obtain

$$\begin{aligned}\int_s^{T_1(\gamma)} e^{\tau-s} x(\tau) d\tau &= \frac{1}{1+e} \left( e^{T_1(\gamma)-s} h - x_1 - \gamma \int_s^{T_1(\gamma)} e^{\tau-s} f(2\omega\tau) d\tau \right), \\ \int_s^{T_1(\gamma)} e^{\tau-s} y(\tau) d\tau &= \frac{1}{1-c} \left( e^{T_1(\gamma)-s} y_2(\gamma) - h \right).\end{aligned}$$

So for  $w_2(\gamma)$  we obtain

$$w_2(\gamma) = e^{-(T_1(\gamma)-s)} \left[ w_1 - \frac{1+c}{1+e} \left( e^{T_1(\gamma)-s} h - x_1 - \gamma \int_s^{T_1(\gamma)} e^{\tau-s} f(2\omega\tau) d\tau \right) + \frac{e-1}{1-c} \left( e^{T_1(\gamma)-s} y_2(\gamma) - h \right) \right],$$

which implies that

$$w_2(0) = \left(\frac{h}{x_1}\right)^{-1/e} \left[ w_1 - \frac{1+c}{1+e} \left( \left(\frac{h}{x_1}\right)^{1/e} h - x_1 \right) + \frac{e-1}{1-c} \left( \left(\frac{h}{x_1}\right)^{1/e-c/e} h - h \right) \right] \approx -\frac{1+c}{1+e} h,$$

and

$$\begin{aligned}w_2'(0) &= -e^{s-T_1(0)} \left[ w_1 - \frac{1+c}{1+e} (e^{-s+T_1(0)} h - x_1) - \frac{1-e}{1-c} (-h + e^{-s+T_1(0)} y_2(0)) \right] T_1'(0) \\ &\quad + e^{s-T_1(0)} \left[ -\frac{1+c}{1+e} \left( -\int_s^{T_1(0)} e^{-s+\tau} f(2\omega\tau) d\tau + e^{-s+T_1(0)} h T_1'(0) \right) \right. \\ &\quad \left. - \frac{1-e}{1-c} \left( e^{-s+T_1(0)} y_2(0) T_1'(0) + e^{-s+T_1(0)} y_2'(0) \right) \right].\end{aligned}\tag{32}$$

Note that the terms involving  $y_2(0)$  and  $e^{-s+T_1(0)} h$  cancel out, and that the terms  $x_1$  and  $w_1$  in the first bracket can be assumed to be far smaller than  $h$ . Hence the most important contributions are the remaining three terms in (32):

$$w_2'(0) \approx -e^{s-T_1(0)} \frac{1-e}{1-c} h T_1'(0) - \frac{1-e}{1-c} y_2'(0) + \frac{1+c}{1+e} h^{-1/e} x_1^{1/e} \int_s^{T_1(0)} e^{-s+\tau} f(2\omega\tau) d\tau.$$

Using (29) and (31), the first term in the above equation is

$$-\left(\frac{h}{x_1}\right)^{-1/e} \frac{1-e}{1-c} h T_1'(0),$$

while the second term is

$$-c \frac{1-e}{1-c} h \left(\frac{h}{x_1}\right)^{c/e} T_1'(0),$$

which is far larger than the first term since  $c/e > 1$  and  $x_1 \ll 1$ . It follows that

$$w_2'(0) \approx -x_1^{-1+c/e} \frac{c(1-e)}{e(1-c)} h^{1-c/e} \int_s^{T_1(0)} e^{-e(\tau-s)} f(2\omega\tau) d\tau + \frac{1+c}{1+e} h^{-1/e} x_1^{1/e} \int_s^{T_1(0)} e^{-s+\tau} f(2\omega\tau) d\tau.$$

Therefore, to summarise

$$T_1(\gamma) = s + \log\left(\frac{h}{x_1}\right)^{1/e} - \gamma \left[ x_1^{-1} \frac{1}{e} \int_s^{T_1(0)} e^{-e(\tau-s)} f(2\omega\tau) d\tau \right] + O(\gamma^2),\tag{33}$$

$$y_2(\gamma) = h^{1-c/e} x_1^{c/e} + \gamma \left[ x_1^{-1+c/e} \frac{c}{e} h^{1-c/e} \int_s^{T_1(0)} e^{-e(\tau-s)} f(2\omega\tau) d\tau \right] + O(\gamma^2),\tag{34}$$

$$z_2(\gamma) = 1 - \frac{1+c}{1+e}h + \gamma \left[ -x_1^{-1+c/e} \frac{c(1-e)}{e(1-c)} h^{1-c/e} \int_s^{T_1(0)} e^{-e(\tau-s)} f(2\omega\tau) d\tau \right. \quad (35)$$

$$\left. + x_1^{1/e} \frac{1+c}{1+e} h^{-1/e} \int_s^{T_1(0)} e^{-s+\tau} f(2\omega\tau) d\tau \right] + O(\gamma^2). \quad (36)$$

## A.2 The global map $H_3^{out} \rightarrow H_1^{in}$

Now we consider the first of the global maps. Suppose that the unstable manifold of  $P'_3$  intersects  $H_3^{out}$  and  $H_1^{in}$  at  $(h, 0, \zeta_2(t, \gamma))$  and  $(\xi_3(t, \gamma), 0, h)$ , respectively. For simplicity, we use  $\zeta_2$  and  $\xi_3$  to denote  $\zeta_2(t, \gamma)$  and  $\xi_3(t, \gamma)$ , and  $\zeta_{20}, \xi_{30}$  to denote  $\zeta_2(T_1(0), 0)$  and  $\xi_3(T_1(0), 0)$  throughout all that follows.

We Taylor expand the diffeomorphism between  $H_3^{out}$  and  $H_1^{in}$  near the point  $(h, 0, \zeta_2(T_1(\gamma), \gamma))$  and suppose that the trajectory starting at  $(h, 0, \zeta_2(t_1, \gamma))$  takes a time  $\delta_1$  to arrive at  $(\xi_3(t_2, \gamma), 0, h)$ . The first order Taylor estimate gives us the affine map  $(h, y_2, z_2) \rightarrow (x_3, y_3, h)$ :

$$\begin{cases} x_3 \approx \xi_3(T_1(\gamma) + \delta_1, \gamma) + A_{111}(T_1(\gamma), \gamma)y_2 + A_{112}(T_1(\gamma), \gamma)(z_2 - \zeta_2(T_1(\gamma), \gamma)) \\ y_3 \approx B_{111}(T_1(\gamma), \gamma)y_2 \end{cases},$$

where  $A_{111}, A_{112}$  and  $B_{111}$  are smooth functions of  $T_1(\gamma)$  and  $\gamma$  which, generically, are non-zero for all small enough  $\gamma$ , and where  $\delta_1$  denotes the time taken to travel from  $H_3^{out}$  to  $H_1^{in}$ . We introduce the additional notation  $A_{110} = A_{111}(T_1(0), 0)$ ,  $A_{120} = A_{112}(T_1(0), 0)$  and  $B_{110} = B_{111}(T_1(0), 0)$ . Substituting (33) - (36) into the above expressions for  $x_3$  and  $y_3$  gives

$$\begin{aligned} x_3 &= \xi_{30} + A_{110}h^{1-c/e}x_1^{c/e} + A_{120} \left( 1 - \frac{1+c}{1+e}h - \zeta_{20} \right) + \gamma \left[ \frac{\partial \xi_3}{\partial \gamma}(T_1(0) + \delta_1, 0) \right. \\ &\quad + \frac{\partial A_{111}}{\partial \gamma}(T_1(0), 0)h^{1-c/e}x_1^{c/e} + \frac{\partial A_{112}}{\partial \gamma}(T_1(0), 0) \left( 1 - \frac{1+c}{1+e}h - \zeta_{20} \right) \\ &\quad - A_{120} \frac{\partial \zeta_2}{\partial \gamma}(T_1(0), 0) - A_{120}x_1^{-1+c/e} \frac{c(1-e)}{e(1-c)} h^{1-c/e} \int_s^{T_1(0)} e^{-e(\tau-s)} f(2\omega\tau) d\tau \\ &\quad \left. + A_{120}x_1^{1/e} \frac{1+c}{1+e} h^{-1/e} \int_s^{T_1(0)} e^{-s+\tau} f(2\omega\tau) d\tau \right] + O(\gamma^2), \end{aligned} \quad (37)$$

and

$$\begin{aligned} y_3 &= B_{110}h^{1-c/e}x_1^{c/e} + \gamma \left[ \left( \frac{\partial B_{111}}{\partial t}(T_1(0), 0)T_1'(0) + \frac{\partial B_{111}}{\partial \gamma}(T_1(0), 0) \right) h^{1-c/e}x_1^{c/e} \right. \\ &\quad \left. + B_{110}x_1^{-1+c/e} \left( \frac{c}{e} \right) h^{1-c/e} \int_s^{T_1(0)} e^{-e(\tau-s)} f(2\omega\tau) d\tau \right] + O(\gamma^2), \end{aligned} \quad (38)$$

where we use the fact that

$$\begin{aligned} \xi_3(T_1(\gamma) + \delta_1, \gamma) &= \xi_{30} + \left[ \frac{\partial \xi_3}{\partial t}(T_1(0) + \delta_1, 0)T_1'(0) + \frac{\partial \xi_3}{\partial \gamma}(T_1(0) + \delta_1, 0) \right] \gamma \\ &= \xi_{30} + \frac{\partial \xi_3}{\partial \gamma}(T_1(0) + \delta_1, 0)\gamma, \end{aligned}$$

since  $\frac{\partial \xi_3}{\partial t}(T_1(0) + \delta_1, 0) = \lim_{\delta \rightarrow 0} [\xi_3(T_1(0) + \delta + \delta_1, 0) - \xi_3(T_1(0) + \delta_1, 0)]/\delta = 0$ , and similarly in other terms. The  $x_1^{c/e}$  terms in (37) can be ignored since  $c/e > 1$  and  $x_1 \ll 1$ . As for (38), using (30), we need to compare the size of  $x_1^{c/e}$  and  $x_1^{-1+c/e} \int_s^{T_1(0)} e^{-e(\tau-s)} f(2\omega\tau) d\tau$ . We observe that, since

$$\int_s^{T_1(0)} e^{-e(\tau-s)} f(2\omega\tau) d\tau \geq \int_s^{s+1} e^{-e(\tau-s)} f(2\omega\tau) d\tau \geq e^{-e} \int_s^{s+1} f(2\omega\tau) d\tau \gg x_1,$$

for small enough  $\gamma$ , the  $x_1^{c/e}$  term in (38) can be ignored. Putting all the leading order and  $O(\gamma)$  terms together, we have

$$x_3 = A_{130} + \gamma \left[ A_{140} - A_{120} x_1^{-1+c/e} \frac{c(1-e)}{e(1-c)} h^{1-c/e} \int_s^{T_1(0)} e^{-e(\tau-s)} f(2\omega\tau) d\tau \right. \\ \left. + A_{120} x_1^{1/e} \frac{1+c}{1+e} h^{-1/e} \int_s^{T_1(0)} e^{-s+\tau} f(2\omega\tau) d\tau \right] + O(\gamma^2), \quad (39)$$

$$y_3 = B_{110} h^{1-c/e} x_1^{c/e} + \gamma B_{110} \left[ x_1^{-1+c/e} \left( \frac{c}{e} \right) h^{1-c/e} \int_s^{T_1(0)} e^{-e(\tau-s)} f(2\omega\tau) d\tau \right] + O(\gamma^2), \quad (40)$$

where  $A_{120}$ ,  $A_{130}$ ,  $A_{140}$  and  $B_{110}$  are constants. Trajectories pass through this point at a time  $T_1(\gamma) + \delta_1$ .

### A.3 The local map $H_1^{in} \rightarrow H_1^{out}$

From this subsection onwards, we will omit most of the details and describe only the main ideas of the calculation. The details are worked out exactly as shown in the previous two subsections. Let  $x(t) = 1 + u(t)$ ,  $x_3 = 1 + u_3$  and  $x_4 = 1 + u_4$ , where  $y_3, u_3 \sim O(\gamma)$ . For a trajectory near the  $P_1(1, 0, 0)$ , the dynamics of the system is approximated by the linearized system

$$\begin{cases} \dot{x} &= \dot{u} = -u - (1+c)y + (e-1)z \\ \dot{y} &= ey \\ \dot{z} &= -cz \end{cases}$$

Integrating the linearised dynamics from  $H_1^{in}$  to  $H_1^{out}$  we obtain the following map from  $H_3^{in}$  to  $H_1^{out}$ , keeping terms up to order  $\gamma$ , as before:

$$\begin{cases} T_2(\gamma) &= s + \delta_1 + \log(B_{110}^{-1} h^{1+c/e} x_1^{-1-c/e})^{1/e} - \gamma \left[ x_1^{-1} \frac{e+c}{e^2} \int_s^{T_1(0)} e^{-e(\tau-s)} f(2\omega\tau) d\tau \right] \\ z_4(\gamma) &= h^{1-c^2/e^2} B_{110}^{c/e} x_1^{c^2/e^2} + \gamma \left[ x_1^{-1+c^2/e^2} B_{110}^{c/e} h^{1-c^2/e^2} \left( \frac{c^2}{e^2} \right) \int_s^{T_1(0)} e^{-e(\tau-s)} f(2\omega\tau) d\tau \right] \\ x_4(\gamma) &= 1 - \frac{1+c}{1+e} h + \gamma \left[ x_1^{-1+c^2/e^2} \frac{c^2(1-e)}{e^2(1-c)} B_{110}^{c/e} h^{1-c^2/e^2} \int_s^{T_1(0)} e^{-e(\tau-s)} f(2\omega\tau) d\tau \right] \end{cases}. \quad (41)$$

### A.4 The global map $H_1^{out} \rightarrow H_2^{in}$

Suppose that the unstable manifold of  $P_1$  intersects  $H_1^{out}$  and  $H_2^{in}$  at  $(\xi_4(t, \gamma), h, 0)$  and  $(h, \eta_5(t, \gamma), 0)$ , where  $\xi_4$  and  $\eta_5$  are smooth functions of  $t$  and  $\gamma$  as before. The affine map  $(x_4, h, z_4) \rightarrow (h, y_5, z_5)$  takes the form

$$\begin{cases} y_5 &= \eta_5(T_2(\gamma) + \delta_2, \gamma) + A_{21}(T_2(\gamma), \gamma)(x_4(\gamma) - \xi_4(T_2(\gamma), \gamma)) + A_{22}(T_2(\gamma), \gamma)z_4(\gamma) + O(\gamma^2) \\ z_5 &= B_{22}(T_2(\gamma), \gamma)z_4(\gamma) + O(\gamma^2) \end{cases},$$

for some coefficients  $A_{21}$ ,  $A_{22}$  and  $B_{22}$  which, generically, are non-zero for all small enough  $\gamma$ . Here  $\delta_2$  denotes the time taken to travel from  $H_1^{out} \rightarrow H_2^{in}$ . Substituting (41) into the above expressions we obtain

$$\begin{cases} y_5(\gamma) &= \eta_{50} + A_{210}(x_4(0) - \xi_{40}) + A_{220}z_4(0) + \gamma \left[ \frac{\partial \eta_5}{\partial \gamma}(T_2(0) + \delta_2, 0) + \frac{\partial A_{21}}{\partial \gamma}(T_2(0), 0)(x_4(0) - \xi_{40}) \right. \\ &\quad \left. + A_{210}(x_4'(0) - \frac{\partial \xi_4}{\partial \gamma}(T_2(0), 0)) + A_{220}z_4'(0) + \frac{\partial A_{22}}{\partial \gamma}(T_2(0), 0)z_4(0) \right] + O(\gamma^2) \\ &= A_{230} + \gamma \left[ A_{24}(T_2(0), 0) + x_1^{-1+c^2/e^2} A_{250} B_{110}^{c/e} h^{1-c^2/e^2} \frac{c^2}{e^2} \int_s^{T_1(0)} e^{-e(\tau-s)} f(2\omega\tau) d\tau \right] + O(\gamma^2) \\ z_5(\gamma) &= B_{220} B_{110}^{c/e} h^{1-c^2/e^2} x_1^{c^2/e^2} + \gamma \left[ \frac{\partial B_{22}}{\partial \gamma}(T_2(0), 0)z_4(0) + B_{220}z_4'(0) \right] + O(\gamma^2) \\ &= B_{220} B_{110}^{c/e} h^{1-c^2/e^2} x_1^{c^2/e^2} + \gamma \left[ x_1^{-1+c^2/e^2} B_{220} B_{110}^{c/e} h^{1-c^2/e^2} \frac{c^2}{e^2} \int_s^{T_1(0)} e^{-e(\tau-s)} f(2\omega\tau) d\tau \right] + O(\gamma^2). \end{cases} \quad (42)$$

Trajectories hit the cross-section  $H_2^{in}$  at time  $t = T_2(\gamma) + \delta_2$ .

### A.5 The local map $H_2^{in} \rightarrow H_2^{out}$

In a similar fashion to before, we let  $y(t) = 1 + v(t)$ ,  $y_5 = 1 + v_5$  and  $y_6 = 1 + v_6$ . The linearized system near  $P_2$  takes the form

$$\begin{cases} \dot{x} &= -cx + f(2\omega t)\gamma \\ \dot{y} &= \dot{v} = -v + (e-1)x - (c+1)z \\ \dot{z} &= ez \end{cases}$$

As in previous subsections, we integrate this linearised system and obtain

$$\begin{cases} T_3(\gamma) &= s + \delta_1 + \delta_2 + \log(B_{220}^{-1}B_{110}^{-1-c/e}h^{1+c/e+c^2/e^2}x_1^{-1-c/e-c^2/e^2})^{1/e} \\ &\quad - \gamma \left[ x_1^{-1} \frac{e^2+ce+c^2}{e^3} \int_s^{T_1(0)} e^{-e(\tau-s)} f(2\omega\tau) d\tau \right] + O(\gamma^2) \\ x_6(\gamma) &= h^{1-c^3/e^3} B_{220}^{c/e} B_{110}^{c^2/e^2} x_1^{c^3/e^3} + \gamma \left[ e^{-c(T_3(0)-T_2(0)-\delta_2)} \int_{T_2(0)+\delta_2}^{T_3(0)} e^{c(\tau-T_2(0)-\delta_2)} f(2\omega\tau) d\tau \right] + O(\gamma^2) \\ y_6(\gamma) &= 1 - \frac{1+c}{1+e}h + \frac{1-e}{1-c}\gamma \left[ e^{-(T_3(0)-T_2(0)-\delta_2)} \int_{T_2(0)+\delta_2}^{T_3(0)} e^{\tau-T_2(0)-\delta_2} f(2\omega\tau) d\tau \right. \\ &\quad \left. - e^{-c(T_3(0)-T_2(0)-\delta_2)} \int_{T_2(0)+\delta_2}^{T_3(0)} e^{c(\tau-T_2(0)-\delta_2)} f(2\omega\tau) d\tau \right] + O(\gamma^2). \end{cases} \quad (43)$$

### A.6 The global map $H_2^{out} \rightarrow H_3^{in}$

We suppose that the unstable manifold of  $P_2'$  intersects  $H_2^{out}$  and  $H_3^{in}$  at  $(\xi_6(t, \gamma), \eta_6(t, \gamma), h)$  and  $(\xi_7(t, \gamma), h, \zeta_7(t, \gamma))$ , respectively. Note that the forms of these two intersection points are slightly different to ones discussed previously since the plane  $\{x = 0\}$  is not invariant. At leading order the map  $(x_6, y_6, h) \rightarrow (x_7, h, y_7)$  takes the form

$$\begin{cases} x_7 &= \xi_7(T_3(\gamma) + \delta_3, \gamma) + A_{31}(T_3(\gamma), \gamma)(x_6(\gamma) - \xi_6(T_3(\gamma), \gamma)) \\ &\quad + A_{32}(T_3(\gamma), \gamma)(y_6(\gamma) - \eta_6(T_3(\gamma), \gamma)) + O(\gamma^2) \\ z_7 &= \zeta_7(T_3(\gamma) + \delta_3, \gamma) + B_{31}(T_3(\gamma), \gamma)(x_6(\gamma) - \xi_6(T_3(\gamma), \gamma)) \\ &\quad + B_{32}(T_3(\gamma), \gamma)(y_6(\gamma) - \eta_6(T_3(\gamma), \gamma)) + O(\gamma^2) \end{cases},$$

where  $A_{31}$ ,  $A_{32}$ ,  $B_{31}$  and  $B_{32}$  are smooth functions both of  $T_3(\gamma)$  and of  $\gamma$  which generically remain non-zero for all small  $\gamma$ .  $\delta_3$  is the time taken to move from  $H_2^{out}$  to  $H_3^{in}$ . Substituting (43) into these expressions we obtain

$$x_7(\gamma) = \mu x_1^{c^3/e^3} + \xi_7(T_3(\gamma) + \delta_3, \gamma) - A_{310}\xi_6(T_3(\gamma), \gamma) + \gamma \left[ A_{310} e^{-c(T_3(0)-T_2(0)-\delta_2)} \int_{T_2(0)+\delta_2}^{T_3(0)} e^{c(\tau-T_2(0)-\delta_2)} f(2\omega\tau) d\tau + \frac{\partial A_{32}}{\partial \gamma} \left( 1 - \frac{1+c}{1+e}h - \eta_{60} \right) \right], \quad (44)$$

where  $\mu$  is a constant which depends only on the form of the perturbation function  $f$ .

Since  $\xi_6$  and  $\xi_7$  are the  $x$ -coordinates of the intersections of the unstable manifold of  $P_2'$  with the cross sections  $H_2^{out}$  and  $H_3^{in}$ , respectively, we may approximate  $\xi_6$  and  $\xi_7$  through affine maps of  $x_{P_2'}$  and  $x_{P_3'}$ , where  $x_{P_2'}$  and  $x_{P_3'}$  denote the  $x$ -coordinates of  $P_2'$  and  $P_3'$ , respectively. It is straightforward to derive that

$$x_{P_2'} = \gamma \frac{1}{e^{c\pi/\omega} - 1} \int_0^{\pi/\omega} e^{c\tau} f(2\omega(t+\tau)) d\tau,$$

and

$$x_{P_3'} = \gamma \frac{1}{e^{-e\pi/\omega} - 1} \int_0^{\pi/\omega} e^{-e\tau} f(2\omega(t+\tau)) d\tau.$$

Therefore

$$\xi_6(t, \gamma) = \lambda_1 + \gamma \lambda_2 \frac{1}{e^{c\pi/\omega} - 1} \int_0^{\pi/\omega} e^{c\tau} f(2\omega(t+\tau)) d\tau, \quad (45)$$

$$\xi_7(t, \gamma) = \lambda_3 \gamma + \gamma \lambda_4 \frac{1}{e^{-e\pi/\omega} - 1} \int_0^{\pi/\omega} e^{-e\tau} f(2\omega(t + \tau)) d\tau, \quad (46)$$

where  $\lambda_1, \lambda_2, \lambda_3$  and  $\lambda_4$  are constants. Substituting (45) and (46) into (44), we have

$$\begin{aligned} x_7(\gamma) = & \mu x_1^{c^3/e^3} + \gamma \left[ \mu_1 + \mu_2 e^{-c(T_3(0)-T_2(0)-\delta_2)} \int_{T_2(0)+\delta_2}^{T_3(0)} e^{c(\tau-T_2(0)-\delta_2)} f(2\omega\tau) d\tau \right. \\ & - \mu_4 \frac{1}{e^{c\pi/\omega} - 1} \int_0^{\pi/\omega} e^{c\tau} f(2\omega(T_3(\gamma) + \tau)) d\tau \\ & \left. - \mu_5 \frac{1}{e^{-e\pi/\omega} - 1} \int_0^{\pi/\omega} e^{-e\tau} f(2\omega(T_3(\gamma) + \delta_3 + \tau)) d\tau \right], \end{aligned}$$

where the  $\mu_j$  are constants. Since neither  $x_7$  nor  $z_7$  depends on  $z_1$  at this order, there is no need to calculate  $z_7$ .

### A.7 The explicit form of the Poincaré map

Since the expression for  $x_7(\gamma)$  depends on  $T_3(\gamma)$  which in turn is given in (43) in terms of  $x_1$  and  $s$ , we have constructed a map from  $(x_1, s) \rightarrow (x_7, T_3 + \delta_3)$  which is our Poincaré map. The map takes the form  $(x, t) \rightarrow (\bar{x}, \bar{t}) = F(x, t) = (f_1(x, t), f_2(x, t)) = (f_1(x, t), t + T(x, t))$ , where

$$\begin{cases} f_1(x, t) &= \mu x^d + \gamma [\mu_1 + \mu_2 L_1(x, t) - \mu_4 G_1(x, t) - \mu_5 G_2(x, t)] + O(\gamma^2), \\ f_2(x, t) &= t + \mu_3 - \xi \log x - \gamma \xi L_2(x, t) x^{-1} + O(\gamma^2), \end{cases} \quad (47)$$

where  $\xi = \frac{e^2 + ce + c^2}{e^3}$ ,  $d = c^3/e^3$ ,  $\mu$  and the  $\mu_j$ s are constants,  $T(x, t)$  denotes the time taken for a point  $(x, t)$  to complete one pass around the whole circuit of cross-sections, and the parts of the map are explicitly given by the expressions

$$L_1(x, t) = e^{-c(T_3(0)-T_2(0)-\delta_2)} \int_{T_2(0)+\delta}^{T_3(0)} e^{c(\tau-T_2(0)-\delta_2)} f(2\omega\tau) d\tau, \quad (48)$$

$$L_2(x, t) = \int_t^{T_1(0)} e^{-e(\tau-t)} f(2\omega\tau) d\tau, \quad (49)$$

$$G_1(x, t) = \frac{1}{e^{c\pi/\omega} - 1} \int_0^{\pi/\omega} e^{c\tau} f(2\omega(T_3(\gamma) + \tau)) d\tau, \quad (50)$$

$$G_2(x, t) = \frac{1}{e^{-e\pi/\omega} - 1} \int_0^{\pi/\omega} e^{-e\tau} f(2\omega(T_3(\gamma) + \delta_3 + \tau)) d\tau. \quad (51)$$

## References

- [1] V.S. Afraimovich and S-B Hsu. *Lectures on Chaotic Dynamical Systems*. American Mathematical Society and International Press, 2002.
- [2] V.S. Afraimovich, S-B Hsu, and H. E. Lin. Chaotic behavior of three competing species of May-Leonard model under small periodic perturbations. *Int. J. Bif. Chaos*, 11(2):435–447, 2001.
- [3] V.S. Afraimovich, M.I. Rabinovich, and P. Varona. Heteroclinic contours in neural ensembles and the winnerless competition principle. *Int. J. Bif. Chaos*, 14, 2004.
- [4] V.S. Afraimovich, V.P. Zhigulin, and M.I. Rabinovich. On the origin of reproducible sequential activity in neural circuits. *Chaos*, 14(4):1123–1129, 2004.

- [5] A.A. Andronov, A.A. Vitt, and S.E. Khaikin. *Theory of Oscillators*. Pergamon, New York, 1996.
- [6] D. Armbruster, J. Guckenheimer, and P. Holmes. Heteroclinic cycles and modulated travelling waves in systems with  $\mathbf{O}(2)$  symmetry. *Physica D*, 29:257–282, 1988.
- [7] P. Ashwin, G. Orosz, J. Wordsworth, and S. Townley. Dynamics on networks of cluster states for globally coupled phase oscillators. *SIAM Journal on Applied Dynamical Systems*, 6(4):728–758, 2007.
- [8] P.L. Boyland. Bifurcations of circle maps: Arnol’d tongues, bistability and rotation intervals. *Commun. Math. Phys.*, 106:353–381, 1986.
- [9] F.H. Busse and K.E. Heikes. Convection in a rotating layer: A simple case of turbulence. *Science*, 208:173–175, 1980.
- [10] P. Chossat and R. Lauterbach *Methods in Equivariant Bifurcations and Dynamical Systems*. Advanced Series in Nonlinear Dynamics, volume 15. World Scientific, 2000.
- [11] P. Couillet, J.M. Gilli, N. Monticelli, and N. Vandenberghe. A damped pendulum forced with a constant torque. *American Journal of Physics*, 73:1122–1128, 2005.
- [12] J.H.P. Dawes, C.M. Postlethwaite, and M.R.E. Proctor. Instabilities induced by a weak breaking of a strong spatial resonance. *Physica D*, 191:1–30, 2004.
- [13] J.H.P. Dawes and T.L. Tsai. Frequency locking and complex dynamics near a periodically forced robust heteroclinic cycle. *Phys. Rev. E*, 74(055201(R)), 2006.
- [14] M. Frean and E.R. Abraham. Rock-scissors-paper and the survival of the weakest. *Proc. R. Soc. Lond. B*, 268:1323–1327, 2001.
- [15] G.A. Gottwald and I. Melbourne. A new test for chaos in deterministic systems. *Proc. R. Soc. Lond. A*, 460:603–611, 2004.
- [16] G.A. Gottwald and I. Melbourne. On the implementation of the 0-1 test for chaos. *SIAM Journal on Applied Dynamical Systems*, 8:129–145, 2009.
- [17] J. Guckenheimer and P. Holmes. Structurally stable heteroclinic cycles. *Math. Proc. Camb. Phil. Soc.*, 103:189–192, 1988.
- [18] J. Hofbauer and K. Sigmund. *Evolutionary Games and Population Dynamics*. Cambridge University Press, Cambridge, U.K., 1998.
- [19] V. Kirk and M. Silber, A competition between heteroclinic cycles. *Nonlinearity* 7:1605–1621, 1994
- [20] V. Kirk and A. M. Rucklidge. The effect of symmetry breaking on the dynamics near a structurally stable heteroclinic cycle between equilibria and a periodic orbit. *Dynamical Systems: An International Journal*, 23(1):43–74, 2008.
- [21] M. Krupa. Robust heteroclinic cycles. *J. Nonlinear Sci.*, 7:129–176, 1997.
- [22] M. Krupa and I. Melbourne. Asymptotic stability of heteroclinic cycles in systems with symmetry. *Erod. Th. & Dynam. Sys.*, 15:121–147, 1997.
- [23] M. Krupa and I. Melbourne. Asymptotic stability of heteroclinic cycles in systems with symmetry, II. *Proc. Roy. Soc. Edinburgh*, 134A:1177–1197, 2004.
- [24] R. Lauterbach. Forced symmetry breaking from  $\mathbf{O}(3)$ . In *Bifurcation and Symmetry*, volume 104, pages 253–262. ISNM, Birkhäuser, Basel, 1992.

- [25] A.J. Lichtenberg and M.A. Lieberman, *Regular and Chaotic Dynamics*. Springer, Applied Mathematical Sciences 38, second edition, 1992.
- [26] R.S. Mackay and C. Tresser. Transition to topological chaos for circle maps. *Physica D*, 19:206–237, 1986.
- [27] R. Mamon, I.P. Malta, M.J. Pacifico, and F. Takens. Rotation intervals of endomorphisms of the circle. *Ergod. Th. & Dynam. Sys.*, 4:493–498, 1984.
- [28] R.M. May and W.J. Leonard. Nonlinear aspects of competition between three species. *SIAM J. Appl. Math.*, 29(2):243–253, 1975.
- [29] S.E. Newhouse, J. Palis, and F. Takens. Bifurcations and stability of families of diffeomorphisms. *I.H.E.S. Publ. Math.*, 57:5–71, 1983.
- [30] M.A. Nowak and K. Sigmund. Evolutionary dynamics of biological games. *Science*, 303:793–799, 2004.
- [31] C.M. Postlethwaite. Stabilization of long-period periodic orbits using time-delayed feedback control. *SIAM J. Appl. Dyn. Syst.*, 8:21–39, 2009
- [32] C.M. Postlethwaite and J.H.P. Dawes. Regular and irregular cycling near a heteroclinic network. *Nonlinearity*, 18:1477–1509, 2005.
- [33] C.M. Postlethwaite and J.H.P. Dawes. A codimension-two resonant bifurcation from a heteroclinic cycle with complex eigenvalues. *Dynamical Systems: An International Journal*, 21:313–336, 2006.
- [34] M.R.E. Proctor and C.A. Jones. The interaction of two spatially resonant patterns in thermal convection. *J. Fluid Mech.*, 188:301–335, 1988.
- [35] M.I. Rabinovich, R. Huerta, and P. Varona. Heteroclinic synchronization: Ultra-subharmonic locking. *Phys. Rev. Lett.*, 96:014101, 2006.
- [36] M.I. Rabinovich, P.V. Varona, A.I. Selverston, and H.D.I. Abarbanel. Dynamical principles in neuroscience. *Reviews of Modern Physics*, 78:1213–1265, 2006.
- [37] M.I. Rabinovich, A. Volkvskii, P. Lecanda, R. Huerta, H.D.I. Abarbanel, and G. Laurent. Dynamical encoding by networks of competing neuron groups: winnerless competition. *Phys. Rev. Lett.*, 87:068102, 2001.
- [38] Y. Sato, E. Akiyama, and J. P. Crutchfield. Stability and diversity in collective adaptation. *Physica D*, 210:21–57, 2005.
- [39] A. Shilnikov, L. Shilnikov, and D. Turaev. On some mathematical topics in classical synchronisation: a tutorial. *Int. J. Bif. Chaos*, 14:2143–2160, 2004.
- [40] E. Stone and P. Holmes. Random perturbations of heteroclinic attractors. *SIAM J. Appl. Math.*, 50(3):726–743, 1990.
- [41] T.L. Tsai and J.H.P. Dawes, Dynamics near a periodically forced robust heteroclinic cycle. *Journal of Physics: Conference Series* 286:012057, 2011.
- [42] P. Varona, R. Levi, Y. I. Arshavsky, M. I. Rabinovich, and A.I. Selverston. Competing sensory neurons and motor rhythm coordination. *Neurocomputing*, 58-60:549–554, 2004.

- [43] P. Varona, M.I. Rabinovich, A.I. Selverston, and Y.I. Arshavsky. Winnerless competition between sensory neurons generates chaos: A possible mechanism for molluscan hunting behavior. *Chaos*, 12:672–677, 2002.
- [44] A. Venaille, P. Varona, and M.I. Rabinovich. Synchronization and coordination of sequences in two neural ensembles. *Phys. Rev. E*, 71:061909, 2005.